

FERMILAB-PUB-21-289-SCD-T, MCNET-21-11

# Coherent QCD Radiation in Vector-Boson-Fusion Higgs Production

Stefan Höche<sup>1</sup>, Stephen Mrenna<sup>1</sup>, Shay Payne<sup>2</sup>, Christian T Preuss<sup>2\*</sup>, Peter Skands<sup>2</sup><sup>1</sup> Fermi National Accelerator Laboratory, Batavia, IL, 60510, USA<sup>2</sup> School of Physics and Astronomy, Monash University, Wellington Road, Clayton, VIC-3800, Australia

\* christian.preuss@monash.edu

June 21, 2021

## 1 Abstract

We discuss the QCD coherence properties of several parton-shower models available in PYTHIA and VINCIA, in the context of Higgs production via vector boson fusion (VBF). The distinctive colour topology of VBF processes allows for the definition of observables that are especially sensitive to the coherent radiation pattern of additional jets. We study a set of such observables, using the VINCIA sector-antenna shower as our main reference, and contrast it to PYTHIA's transverse-momentum-ordered DGLAP shower as well as PYTHIA's dipole-improved shower. We then investigate the robustness of these predictions as successive levels of higher-order perturbative matrix elements are incorporated, including next-to-leading-order matched and tree-level merged calculations, using POWHEG BOX and SHERPA respectively to generate the hard events.

12

## 13 Contents

14	<b>1 Introduction</b>	<b>2</b>
15	<b>2 Setup of the Simulation</b>	<b>4</b>
16	2.1 Hard Process	5
17	2.2 Showers	6
18	2.3 Matching and Merging	7
19	2.3.1 POWHEG Matching	7
20	2.3.2 CKKW-L Merging	8
21	2.4 Analysis	9
22	<b>3 Results</b>	<b>10</b>
23	3.1 Leading Order	11
24	3.2 Next-to-Leading Order Matched	14
25	3.3 Comparison of Matching and Merging	17
26	3.4 Merged with up to Four Jets	20
27	3.5 Hadronisation and Multi-Parton Interactions	21
28	<b>4 Conclusion</b>	<b>22</b>
29	<b>A POWHEG+VINCIA Setup</b>	<b>25</b>

30 **B VINCIA CKKW-L Setup**

26

31 **References**

27

32

33

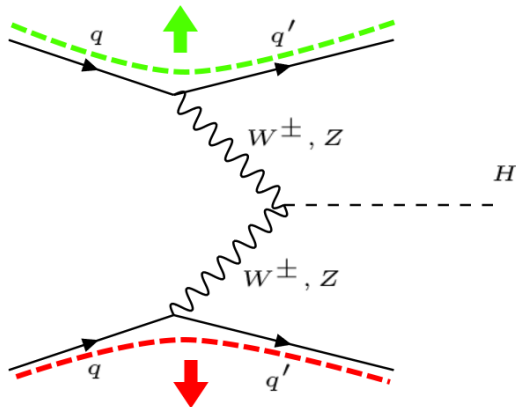


Figure 1: QCD colour flow of the LO VBF Higgs production process. Due to the kinematics of the interaction, QCD radiation is directed in the forward region of the detector.

34 **1 Introduction**

35 Higgs boson production via Vector Boson Fusion (VBF) — fig. 1 — is among the most im-  
 36 portant channels for Higgs studies at the Large Hadron Collider (LHC). With a Standard-  
 37 Model (SM) cross section of a few pb at LHC energies, VBF accounts for order 10% of  
 38 the total LHC Higgs production rate [1]. The modest rate is compensated for by the  
 39 signature feature of VBF processes: two highly energetic jets generated by the scattered  
 40 quarks, in the forward and backward regions of the detector respectively, which can be  
 41 tagged experimentally and used to significantly reduce background rates. Moreover, the  
 42 unique colour flow of the VBF process, highlighted by the coloured thick dashed lines in  
 43 fig. 1, strongly suppresses any coherent Bremsstrahlung into the central region, leaving  
 44 this region comparatively clean and well suited for precision studies of the Higgs boson  
 45 decay products. With over half a million Higgs bosons produced in the VBF channel in  
 46 total during Run II of the LHC and a projection that this will more than double during  
 47 Run III, studies of this process have already well and truly entered the realm of precision  
 48 physics.

49 On the theory side, the current state of the art for the  $H + 2j$  process in fixed-order  
 50 perturbation theory is inclusive next-to-next-to-next-to-leading order QCD [2], fully differ-  
 51 ential next-to-next-to-leading order (NNLO) QCD [3–6] and next-to-leading-order (NLO)  
 52 electroweak (EW) calculations [7]. These calculations of course only offer their full pre-  
 53 cision for observables that are non-zero already at the Born level, such as the total cross  
 54 section and differential distributions of the Higgs boson and tagging jets. For more ex-  
 55 clusive event properties, such as Bremsstrahlung and hadronisation corrections, the most  
 56 detailed description is offered by combinations of fixed-order and parton-shower calcula-  
 57 tions. To this end, two recent phenomenological studies [8, 9] compared different NLO+PS  
 58 simulations among each other as well as to NLO and NNLO calculations. These compara-

59 tive studies catered to two needs; firstly, the reliability of matched calculations was tested  
 60 in regions where resummation effects are small. Furthermore, a more realistic estimate of  
 61 parton-shower as well as matching uncertainties was obtained by means of different shower  
 62 and matching methods in independent implementations.

63 The earlier of the two studies [10] highlighted that different NLO+PS implementations  
 64 describe the intrinsically coherent radiation in this process quite differently, and that the  
 65 uncertainties arising from the choice of the shower and matching implementation can per-  
 66 sist even at the NLO-matched level. Among its central results, the study [10] found that  
 67 PYTHIA's default shower [11–13] describes the emission pattern of the third jet poorly, es-  
 68 sentially missing the coherence of the initial-final dipoles. This effect was most pronounced  
 69 for MADGRAPH\_AMC@NLO [14] + PYTHIA, for which a global recoil scheme must be used  
 70 in both the time-like and space-like shower in order to match the subtraction terms im-  
 71 plemented in MADGRAPH\_AMC@NLO. For POWHEG-BOX [15] + PYTHIA, the difference  
 72 persisted when using the global recoil scheme<sup>1</sup>. However, changing to PYTHIA's alterna-  
 73 tive dipole-recoil scheme [16], which should reproduce coherence effects more faithfully,  
 74 improved the agreement, both with calculations starting from  $H + 3j$  as well as with the  
 75 angular-ordered coherent shower model in HERWIG 7 [17].

76 The more recent study [9] highlighted a number of interesting aspects of vector boson  
 77 fusion that can be exploited to enhance the signal-to-background ratio in future measure-  
 78 ments: Firstly, if the Higgs boson is boosted, the  $t$ -channel structure of the VBF matrix  
 79 elements leads to less QCD radiation when compared to the irreducible background from  
 80 gluon-gluon fusion. Secondly, it was found that a global jet veto provides a similarly ef-  
 81 fective cut as a central jet veto, leading to much reduced theoretical uncertainties, and  
 82 in particular eliminating the need to resum non-global logarithms associated with inhib-  
 83 ited radiation in the rapidity gap. Despite a good overall agreement between fixed-order  
 84 NNLO and NLO-matched parton shower predictions, the study also pointed out a few  
 85 subtle disagreements for highly boosted Higgs boson topologies. In these scenarios, the  
 86 standard fixed-order paradigm of operating with a single factorisation scale is no longer  
 87 appropriate, because higher-order corrections should be resummed individually for the two  
 88 impact factors in the structure-function approach.

89 The uncertainties arising from matching systematics in vector-boson-fusion and vector-  
 90 boson-scattering processes (VBS) have also been studied in the past [18] with rather good  
 91 agreement between different showers at the level of  $H + 3j$  NLO+PS calculations [8],  
 92 although in that study, only the POWHEG matching scheme was considered. Very recently,  
 93 an extensive review [19] collected experimental results and theoretical developments in  
 94 VBS processes in view of the high-luminosity upgrade of the LHC as well as future colliders.

95 On the experimental side, recent studies of VBF Higgs production by ATLAS [20, 21]  
 96 and CMS [22, 23] have used PYTHIA's default shower model matched to the NLO via the  
 97 POWHEG technique, with only one of them [20] employing PYTHIA's dipole option. The  
 98 associated modelling uncertainties, and ways to reduce them, therefore remain of high  
 99 current relevance.

100 We extend the comparative study of [10] to include the new coherent VINCIA sector-  
 101 antenna shower [24] that has become available starting from PYTHIA version 8.304. We also  
 102 consider two new observables designed to further probe the amount of coherent radiation  
 103 by measuring the summed transverse energy  $H_T$  for  $|\eta| < 0.5$  and for  $|\eta - \eta_0| < 0.5$   
 104 respectively, where  $\eta_0$  is the midpoint between the two tagging jets. To investigate the  
 105 robustness of the predictions, we include not only POWHEG-BOX + PYTHIA [13, 15] but  
 106 also a new dedicated implementation of the CKKW-L merging scheme [25–27] for sector

<sup>1</sup>We note that the global recoil scheme is the default choice only for PYTHIA's space-like DGLAP shower, while the time-like DGLAP shower uses a dipole-like recoil scheme per default.

107 showers [28], with hard events with up to four additional jets generated by SHERPA 2 [29,  
 108 30]. We emphasise that this is currently the only multi-jet merging approach in PYTHIA 8.3  
 109 which can handle VBF processes<sup>2</sup>. Additionally, we highlight the systematic uncertainties  
 110 arising from the use of vetoed showers in the POWHEG scheme and make recommendations  
 111 for settings related to the use of these in PYTHIA.

112 This study is structured as follows. We begin with an overview of the setup for our  
 113 simulations in section 2; starting with an overview of the fixed order, shower, matched  
 114 and merged calculations and leading towards a description of the analysis we perform. We  
 115 then move on to discuss the results of our analysis in section 3, with our conclusions and  
 116 recommendations listed in section 4.

## 117 2 Setup of the Simulation

118 We consider Higgs production via VBF in proton-proton collisions at the high-luminosity  
 119 LHC with a centre-of-mass energy of  $\sqrt{s} = 14$  TeV.

120 The simulation is factorised into the generation of the hard process using SHERPA  
 121 2 (for the LO merging samples) and POWHEG-BOX v2 (for the NLO matched samples)  
 122 and subsequent showering with PYTHIA 8.306. A cross check is also performed using  
 123 PYTHIA’s internal Born-level VBF process. Details on the hard-process setups are given  
 124 in section 2.1.

125 Since we expect the VINCIA antenna shower to account for coherence more faithfully  
 126 than does PYTHIA’s default “simple”  $p_{\perp}$ -ordered DGLAP shower, we take VINCIA’s descrip-  
 127 tion as the baseline for our comparisons, contrasting it to PYTHIA’s default and “dipole-  
 128 recoil” options. Details on the shower setups are given in section 2.2.

129 Higher fixed-order corrections are taken into account at NLO+PS accuracy via the  
 130 POWHEG scheme, and for VINCIA also in the CKKW-L scheme up to  $\mathcal{O}(\alpha_S^4)$ . We expect  
 131 that these corrections will be smaller for coherent shower models than for incoherent ones,  
 132 hence these comparisons serve both to test the reliability of the baseline showers and to  
 133 illustrate any ambiguities that remain after these corrections are included. Details on the  
 134 matching and merging setups are given in section 2.3.

135 Finally, in section 2.4, we define the observables and the VBF analysis cuts that are  
 136 used for the numerical studies in section 3.

137 Note that, since we are primarily interested in exploring the coherence properties of  
 138 the perturbative stages of the event simulation, most of the results will be at the so-called  
 139 “parton level”, i.e. without accounting for non-perturbative or non-factorisable effects  
 140 such as hadronisation, primordial  $k_T$ , or multi-parton interactions (MPI). Although this  
 141 is not directly comparable to physical measurements (nor is the definition universal since  
 142 different shower models define the cutoff differently), the factorised nature of the infrared  
 143 and collinear safe observables we consider imply that, while non-perturbative effects may  
 144 act to smear out the perturbative differences and uncertainties, they would not in general  
 145 be able to obviate them, thus making studies of the perturbative stages interesting in  
 146 their own right. Nevertheless, with jet  $p_T$  values going down to 25 GeV and  $H_T$  being  
 147 sensitive to the overall amount of energy scattered into the central region, we include  
 148 further comparisons illustrating the effect of non-perturbative corrections at the end of  
 149 section 3.

---

<sup>2</sup>We do note that a technical (but unphysical) fix was introduced in PYTHIA 8.242 and is planned to be re-implemented in a future version of PYTHIA 8.3.

## 150 2.1 Hard Process

151 For the parton-level event generation, we use a stable Higgs boson with a mass of  $M_H =$   
 152  $125 \text{ GeV}$ , and we set the electroweak boson masses and widths to

$$\begin{aligned} M_Z &= 91.1876 \text{ GeV}, & \Gamma_Z &= 2.4952 \text{ GeV}, \\ M_W &= 80.385 \text{ GeV}, & \Gamma_W &= 2.085 \text{ GeV}. \end{aligned} \quad (1)$$

153 Electroweak parameters are derived from this set with the additional input of the elec-  
 154 tromagnetic coupling constant at the  $Z$  pole ( $\alpha(M_Z)$  scheme, `EW_SCHEME = 2` in SHERPA):

$$155 \frac{1}{\alpha(M_Z)} = 128.802. \quad (2)$$

156 We treat all flavours including the bottom quark as massless and use a diagonal CKM  
 157 mixing matrix. In both SHERPA and POWHEG-BOX, we use the `CT14_NNLO_as118` [31] PDF  
 158 set provided by LHAPDF6 [32] with the corresponding value of  $\alpha_S$ . For the sample generated  
 159 with PYTHIA's internal VBF implementation, we use its default `NNPDF23_lo_as_0130_qed`  
 160 PDF set [33, 34].

161 Tree-level event samples with up to four additional jets are generated using an HPC-  
 162 enabled variant of SHERPA 2 [29, 30], utilising the COMIX matrix-element generator [35].  
 163 To facilitate efficient parallelised event generation and further processing, events are stored  
 164 in the binary HDF5 data format [30]. The factorisation and renormalisation scales are  
 165 chosen to be

$$\mu_F^2 = \mu_R^2 = \frac{\hat{H}_T^2}{4} \quad \text{with} \quad \hat{H}_T = \sum_j p_{T,j} + \sqrt{M_H^2 + p_{T,H}^2}. \quad (3)$$

166 and jets are defined according to the  $k_T$  clustering algorithm with  $R = 0.4$  and a cut at  
 167  $20 \text{ GeV}$ .

168 PYTHIA's internal events are generated with scales governed by the two switches  
 169 `SigmaProcess:factorScale3VV` and `SigmaProcess:renormScale3VV`, respectively. Their  
 170 default values = 2 and = 3, respectively, correspond to the choices

$$\mu_F^2 = \sqrt{m_{T,V_1}^2 m_{T,V_2}^2} \equiv \sqrt{(M_{V_1}^2 + p_{T,q_1}^2)(M_{V_2}^2 + p_{T,q_2}^2)}, \quad (4)$$

$$\mu_R^2 = \sqrt{m_{T,V_1}^2 m_{T,V_2}^2 m_{T,H}^2} \equiv \sqrt[3]{(M_{V_1}^2 + p_{T,q_1}^2)(M_{V_2}^2 + p_{T,q_2}^2)m_{T,H}^2}, \quad (5)$$

171 with the pole masses of the exchanged vector bosons  $M_{V_1}$ ,  $M_{V_2}$ , the transverse mass of  
 172 the Higgs boson  $m_{T,H}$ , and the transverse momenta of the two final-state quarks  $p_{T,q_1}$ ,  
 173  $p_{T,q_2}$ .

174 For NLO calculations matched to parton showers, we consider the POWHEG [36, 37]  
 175 formalism. POWHEG samples are generated with POWHEG-BOX v2 [15, 38] with the fac-  
 176 torisation and renormalisation scales chosen as

$$\mu_F^2 = \mu_R^2 = \frac{M_H}{2} \sqrt{\left(\frac{M_H}{2}\right)^2 + p_{T,H}^2}. \quad (6)$$

177 Since the study in [10] did not find any significant effect from the choice of the “`hdamp`”  
 178 parameter in POWHEG, we do not include any such damping here, corresponding to a  
 179 choice of `hdamp = 1`.

## 180 2.2 Showers

181 The hard events defined above are showered with the three following shower models, which  
182 are all available in PYTHIA 8.306:

- 183 • VINCIA’s sector antenna shower [24]. The “sector” mode is the default option for  
184 VINCIA since PYTHIA 8.304 and also enables us to make use of VINCIA’s efficient  
185 CKKW-L merging [28]. We expect it to exhibit the same level of coherence as the  
186 fixed-order matrix elements, at least at leading colour (LC), since its QCD antenna  
187 functions and corresponding phase-space factorisations explicitly incorporate the  
188 soft-eikonal function for all possible (LC) colour flows. Of particular relevance to  
189 this study is its coherent treatment of “initial-final” (IF) colour flows.
- 190 • PYTHIA’s default “simple shower” model [11,12], which implements  $p_T$ -ordered DGLAP  
191 evolution with dipole-style kinematics. For IF colour flows, however, the kinematic  
192 dipoles are not identical to the colour dipoles, and this can impact coherence-sensitive  
193 observables [39].
- 194 • PYTHIA’s “simple shower” with the dipole-recoil option [16]. Despite its name, this  
195 not only changes the recoil scheme; in fact, it replaces the two independent DGLAP  
196 evolutions of IF dipoles by a coherent, antenna-like, dipole evolution, while keeping  
197 the DGLAP evolution of other dipoles unchanged. This option should therefore lead  
198 to radiation patterns exhibiting a similar level of coherence as VINCIA.

199 Ordinarily, PYTHIA would of course also add decays of the Higgs boson, and any final-  
200 state radiation associated with that. However, as a colour-singlet scalar with  $\Gamma_H \ll \Lambda_{\text{QCD}}$   
201 and  $\Gamma_H/M_H \sim \mathcal{O}(10^{-5})$ , its decay can be treated as factorised from the production process  
202 to a truly excellent approximation. For the purpose of this study, we therefore keep  
203 the Higgs boson stable, to be able to focus solely on the radiation patterns of the VBF  
204 production process itself, without the complication of decay products in the central region.

205 For all of the shower models, we retain PYTHIA’s default PDF choice<sup>3</sup>, regardless of  
206 which PDF set was used to generate the hard process. This is done to remain consistent  
207 with the default shower tunings [40] and due to the better-controlled backwards-evolution  
208 properties of the default set [41].

209 Per default, the shower starting scale is chosen to be the factorisation scale of the hard  
210 process,

$$\mu_{\text{PS}}^2 = \mu_{\text{F}}^2. \quad (7)$$

211 In VINCIA, this scale can be varied by a multiplicative “fudge” factor, controlled by  
212 `Vincia:pTmaxFudge`,

$$\mu_{\text{PS}}^2 = k_{\text{fudge}} \mu_{\text{F}}^2,$$

213 while in PYTHIA, the starting scales of the initial-state and final-state showers can be  
214 varied independently,

$$\begin{aligned} \mu_{\text{PS,FSR}}^2 &= k_{\text{fudge,FSR}} \mu_{\text{F}}^2, \\ \mu_{\text{PS,ISR}}^2 &= k_{\text{fudge,ISR}} \mu_{\text{F}}^2, \end{aligned}$$

215 controlled by `TimeShower:pTmaxFudge` and `SpaceShower:pTmaxFudge`, respectively.

216 In a similar vein, the strong coupling in the shower is evaluated at the shower  $p_T$ -  
217 scale, modified by renormalisation-scale factors  $k_{\text{ren}}$ . In PYTHIA, the strong coupling at

---

<sup>3</sup>NNPDF23\_lo\_as\_0130\_qed.

218 the  $Z$  mass is set to  $\alpha_S(M_Z) = 0.1365$  and independent scale factors for ISR and FSR are  
 219 implemented,

$$\alpha_S^{\text{Pythia,FSR}}(p_{\perp\text{evol,FSR}}^2) = \alpha_S^{\overline{\text{MS}}}(k_{\text{R,FSR}} p_{\perp\text{evol,FSR}}^2),$$

$$\alpha_S^{\text{Pythia,ISR}}(p_{\perp\text{evol,ISR}}^2) = \alpha_S^{\overline{\text{MS}}}(k_{\text{R,ISR}} p_{\perp\text{evol,ISR}}^2).$$

220 These can be set via `TimeShower:renormMultFac` and `SpaceShower:renormMultFac`,  
 221 respectively, and are unity by default. The transverse-momentum evolution variables  
 222  $p_{\perp\text{evol,FSR}}^2$  and  $p_{\perp\text{evol,ISR}}^2$  are defined as in [11].

223 For VINCIA, on the other hand, a more refined choice can be made with separate renor-  
 224 malisation factors being implemented for (initial- and final-state) emissions, (initial- and  
 225 final-state) gluon splittings, and (initial-state) quark conversions. These have the default  
 226 settings:

$$k_{\text{R,Emit}}^{\text{F}} = 0.66, \quad k_{\text{R,Split}}^{\text{F}} = 0.8,$$

$$k_{\text{R,Emit}}^{\text{I}} = 0.66, \quad k_{\text{R,Split}}^{\text{I}} = 0.5, \quad k_{\text{R,Conv}}^{\text{I}} = 0.5,$$

227 which can be set via the parameters

```
228 Vincia:renormMultFacEmitF
Vincia:renormMultFacSplitF
Vincia:renormMultFacEmitI
Vincia:renormMultFacSplitI
Vincia:renormMultFacConvI.
```

229 Additionally, VINCIA uses the CMW scheme [42] (while PYTHIA does not), i.e. it evaluates  
 230 the strong coupling according to

$$\alpha_S^{\text{CMW}} = \alpha_S^{\overline{\text{MS}}} \left( 1 + \frac{\alpha_S^{\overline{\text{MS}}}}{2\pi} \left[ C_A \left( \frac{67}{18} - \frac{\pi^2}{6} \right) - \frac{5n_f}{9} \right] \right), \quad (8)$$

231 where  $\alpha_S^{\overline{\text{MS}}}(M_Z) = 0.118$ , so that

$$\alpha_S^{\text{Vincia}}(p_{\perp}^2) = \alpha_S^{\text{CMW}}(k_{\text{R}} p_{\perp}^2) \quad (9)$$

232 with the VINCIA evolution variable as defined in [24].

## 233 2.3 Matching and Merging

234 In the following, we will briefly review the defining features of the POWHEG NLO matching  
 235 and the CKKW-L merging schemes we will use in this study. In particular, we will focus  
 236 on the technicalities and practicalities to ensure a consistent use. Detailed reviews of the  
 237 POWHEG schemes can for instance be found in [43] and [44]. The CKKW-L scheme is  
 238 explained in detail in [27] and its extension to the VINCIA sector shower in [28].

### 239 2.3.1 POWHEG Matching

240 In the POWHEG formalism, events are generated according to the inclusive NLO cross  
 241 section with the first emission generated according to a matrix-element corrected no-  
 242 emission probability.

243 Since the shower kernels in the POWHEG no-emission probability are replaced by the  
 244 ratio of the real-radiation matrix element to the Born-level one, it is independent of the  
 245 shower it will later be matched to. It is, however, important to stress that generally,



246 the POWHEG ordering variable will not coincide with the ordering variable of the shower.  
 247 Starting a shower with a different ordering variable at the POWHEG scale of the first emis-  
 248 sion might thus lead to over- or undercounting emissions. A simple method to circumvent  
 249 this was presented in [45]. There, the shower is started at the phase space maximum  
 250 (a so-called “power shower” [46]) and emissions harder than the POWHEG one are vetoed  
 251 until the shower reaches a scale below the scale of the first emission. For general ordering  
 252 variables, there is, however, no guarantee that once the shower falls below the scale of  
 253 the POWHEG emission it will not generate a harder emission later on in the evolution.  
 254 This is especially important if the shower is not ordered in a measure of hardness but  
 255 e.g. in emission angles, such as the HERWIG  $\tilde{q}$  shower [47]. In these cases, it is advisable  
 256 to recluster the POWHEG emission and start a truncated and vetoed shower off the Born  
 257 state [36]. This scheme also avoids the issue that in vetoed showers, all emissions in the  
 258 shower off a Born+1-jet state are compared against the POWHEG emission as if they were  
 259 the first emission themselves. But from the point of view of kinematics and colour they  
 260 will still be the second, third, etc.

261 However, since all showers we consider here are ordered in a notion of transverse  
 262 momentum, it shall suffice for our purposes to use the simpler “vetoed power shower”  
 263 scheme. To this end, we have amended the existing POWHEG user hook for PYTHIA’s  
 264 showers by a dedicated one for POWHEG+VINCIA, which has been included in the standard  
 265 release of PYTHIA starting from version 8.306; see appendix A for detailed instructions.

266 For both PYTHIA and VINCIA, we use a vetoed shower with the POWHEG  $p_T$  and  
 267  $d_{ij}$  definitions, corresponding to the mode `POWHEG:pTdef = 1`. We define the POWHEG  
 268 scale with respect to the radiating leg and use PYTHIA’s definition of emitter and recoiler,  
 269 corresponding to the modes `POWHEG:pTemt = 0` and `POWHEG:emitted = 0`. Per default,  
 270 we choose to define the scale of the POWHEG emission by the minimum  $p_T$  among all  
 271 final-state particles, i.e. use `POWHEG:pThard = 2`, according to the suggestion in [48]. As  
 272 an estimate of the uncertainty of this choice, we vary the  $p_{T,\text{hard}}$  scale to be the LHEF  
 273 scale and the  $p_T$  of the POWHEG emission, corresponding to the modes `POWHEG:pThard =`  
 274 `0` and `POWHEG:pThard = 1`, respectively.

275 The purpose of these settings is to ensure maximally consistent scale definitions while  
 276 not reverting to the (more involved) “truncated and vetoed shower” scheme mentioned  
 277 above. While we deem the choices made here appropriate for the case at hand they remain  
 278 ambiguous, effectively introducing systematic matching uncertainties into the (precision)  
 279 calculation. As a means of estimating these uncertainties, we will discuss the influence of  
 280 the  $p_{T,\text{hard}}$  scale setting on physical observables below in section 3.

### 281 2.3.2 CKKW-L Merging

282 Multi-leg merging schemes aim at correcting parton shower predictions away from the soft  
 283 and collinear regions. In the CKKW-L merging scheme [27], multiple inclusive tree-level  
 284 event samples are combined to a single inclusive one by introducing a (somewhat arbitrary)  
 285 “merging scale”  $t_{\text{MS}}$  which separates the matrix-element ( $t > t_{\text{MS}}$ ) from the parton-shower  
 286 ( $t < t_{\text{MS}}$ ) region. In this way, over-counting of emissions is avoided while accurate parton-  
 287 shower resummation in logarithmically enhanced regions and leading-order accuracy in the  
 288 regions of hard, well-separated jets is ensured if the merging scale is chosen appropriately.

289 The missing Sudakov suppression in higher-multiplicity configurations is calculated  
 290 post-facto by the use of truncated trial showers between the nodes of the most probable  
 291 “shower history”. In this context, the shower history represents the sequence of interme-  
 292 diate states the parton shower at hand would (most probably) have generated to arrive  
 293 at the given  $n$ -jet state. Usually, this sequence is constructed by first finding all possible  
 294 shower histories and subsequently choosing the one that maximises the branching proba-



295 bility, i.e., the product of branching kernels and the Born matrix element. As we employ  
 296 this scheme with VINCIA’s sector shower, a few comments are in order. The objective of  
 297 the sector shower is to replace the probabilistic shower history by a deterministic history,  
 298 governed by the singularity structure of the matrix element. This means that at each  
 299 point in phase space only the most singular branching contributes. In the shower, this is  
 300 ensured by vetoing any branchings that do not abide by this; in the merging, this results  
 301 in a faster and less resource-intensive algorithm, as it is no longer required to generate a  
 302 large number of possible histories. Details and subtleties of VINCIA’s sectorised CKKW-L  
 303 implementation can be found in [28].

304 The CKKW-L merging scheme is in principle implemented for all showers in PYTHIA  
 305 8.3. However, the intricate event topology of VBF processes currently prohibits the use  
 306 of PYTHIA’s default merging implementation<sup>4</sup>. We hence limit ourselves to study the  
 307 effect of merging with VINCIA, and have adapted VINCIA’s CKKW-L implementation [28]  
 308 so that VBF processes are consistently treated. Specifically, the flag `Vincia:MergeVBF =`  
 309 `on` should be used, which restricts the merging to only consider shower histories that retain  
 310 exactly two initial-final quark lines. As a consequence, there must not be any “incomplete  
 311 histories” (histories that do not cluster back to a VBF Born configuration); this should be  
 312 guaranteed as long as the input event samples are of the VBF type only and no QED or  
 313 EW emissions are generated. A complete list of relevant settings for the use of VINCIA’s  
 314 CKKW-L merging is collected in appendix B.

## 315 2.4 Analysis

316 We use the anti- $k_T$  algorithm [49] with  $R = 0.4$ , as implemented in the FASTJET [50]  
 317 package, to cluster jets in the range,

$$p_T > 25 \text{ GeV}, \quad |\eta| < 4.5.$$

318 In addition, we employ typical VBF cuts to ensure that the two “tagging jets” are suffi-  
 319 ciently hard, have a large separation in pseudorapidity, and are located in opposite hemi-  
 320 spheres:

$$m_{j_1, j_2} \geq 600 \text{ GeV}, \quad |\Delta\eta_{j_1, j_2}| \geq 4.5, \quad \eta_{j_1} \cdot \eta_{j_2} \leq 0.$$

321 We consider the following observables:

- 322 • **Pseudorapidity Distributions:** at the Born level, the two tagging jets already  
 323 have nontrivial pseudorapidity distributions. These are sensitive to showering chiefly  
 324 via recoil effects and via the enhancement of radiation towards the beam directions.  
 325 The third (and subsequent) jets are of course directly sensitive to the generated  
 326 emission spectra. To minimise contamination from final-state radiation off the tag-  
 327 ging jets, we also consider the pseudorapidity of the radiated jet(s) relative to the  
 328 midpoint of the two tagging jets,

$$\eta_{j_i}^* = \eta_{j_i} - \eta_0, \tag{10}$$

329 with the midpoint defined by:

$$\eta_0 = \frac{1}{2}(\eta_{j_1} + \eta_{j_2}). \tag{11}$$

- 330 • **Transverse Momentum Distributions:** we expect coherence effects for the ra-  
 331 diated jets ( $i > 2$ ) to be particularly pronounced for radiation that is relatively

---

<sup>4</sup>We note that a technical fix for this was available in PYTHIA 8.245 and will become available again in PYTHIA 8.3 in the future.

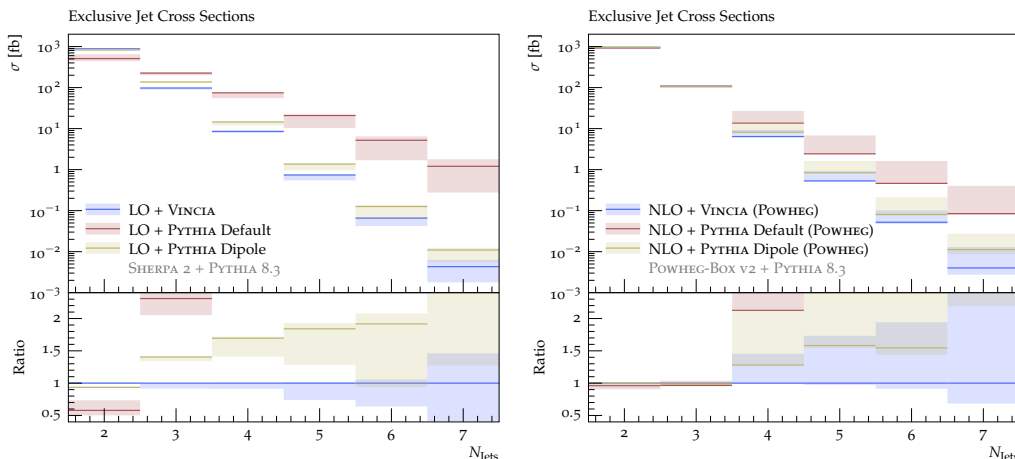


Figure 2: Exclusive jet cross sections at LO+PS (*left*) and POWHEG NLO+PS (*right*) accuracy. The bands are obtained by a variation of the default shower scale by a factor of two or the variation of the hard scale, respectively.

332 soft in comparison to the characteristic scale of the hard process. Conversely, the  
 333 transverse momenta of the two tagging jets should mainly be affected indirectly, via  
 334 momentum-conservation (recoil) effects.

335 • **Scalar Transverse Momentum Sum:** as a more inclusive measure of the summed  
 336 jet activity in the central rapidity region, we consider the scalar transverse momen-  
 337 tum sum of all reconstructed jets (defined as above, i.e., with  $p_T > 25 \text{ GeV}$ ),

$$H_T = \sum_j |p_{T,j}|, \quad (12)$$

338 in two particular regions:

- 339 – in the central rapidity region,  $\eta \in [-\frac{1}{2}, +\frac{1}{2}]$
- 340 – around the midpoint of the tagging jets,  $\eta^* \in [-\frac{1}{2}, +\frac{1}{2}]$ , cf eq. (10).

341 We point out that, due to the way it is constructed, the second of these regions is not  
 342 sensitive to the tagging jets, as it is not possible for them to fall within this region.  
 343 Unlike the previous two observables,  $H_T$  is sensitive to the overall radiation effect in  
 344 the given region, not just that of a certain jet multiplicity. As such, we expect  $H_T$   
 345 to give a measure of the all-orders radiation effects.

346 The analysis is performed using the RIVET analysis framework [51, 52] and based on the  
 347 one used in [10].

### 348 3 Results

349 In this section, we present the main results of our study based on the setup described in  
 350 the last section. In fig. 2, the exclusive jet cross sections for up to 7 jets are shown at  
 351 LO+PS and NLO+PS (via the POWHEG scheme) accuracy at the Born level. While there  
 352 are very large differences between the three shower predictions at the leading order, there  
 353 is good agreement between the NLO+PS predictions at least for the 2- and 3-jet cross  
 354 sections.

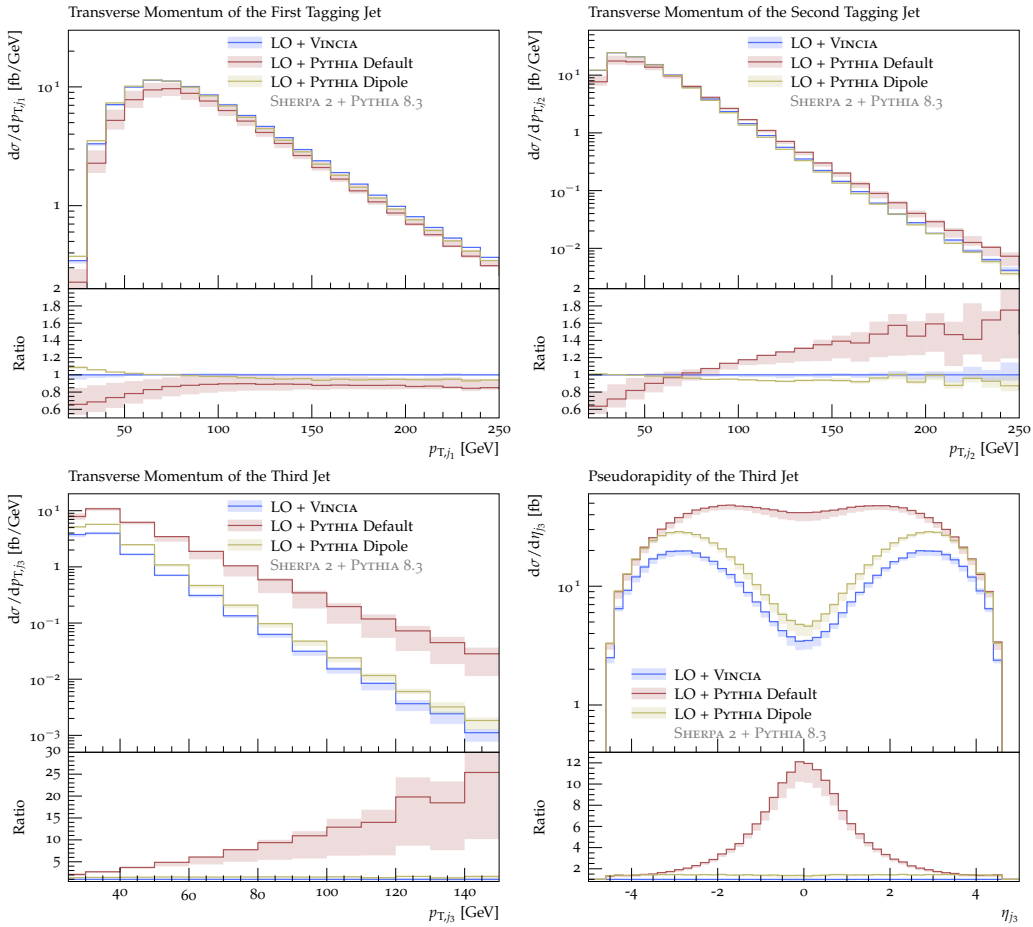


Figure 3: Transverse momentum of the first tagging jet (*top left*), second tagging jet (*top right*), third jet (*bottom left*), and pseudorapidity of the third jet (*bottom right*) at LO+PS accuracy. The bands are obtained by a variation of the default shower starting scale by a factor of two.

### 3.1 Leading Order

It is instructive to start by studying the properties of the baseline leading-order + shower calculations, without including higher fixed-order corrections.

We use the leading-order event samples generated with SHERPA and by default let the factorisation scale  $\mu_F^2$  define the shower starting scale. As a way to estimate the uncertainty associated with this choice, we vary the shower starting scale  $\mu_{PS}^2$  by a factor  $k_{\text{fudge}} \in [\frac{1}{2}, 2]$ ,  $\mu_{PS}^2 = k_{\text{fudge}} \mu_F^2$ . Strictly speaking, shower starting scales not equal to the factorisation scale lead to additional PDF ratios in the no-branching probabilities generated by the shower, but for factor-2 variations these are consistent with unity (since the PDF evolution is logarithmic) and we therefore neglect them. Compared to the shower starting scale, variations of the shower renormalisation scale only have a marginal effect and are therefore not shown here. As we are primarily concerned with the shower radiation patterns, we do not vary the scales in the fixed-order calculation. The effect of those variations have been studied extensively in the literature before, cf. e.g. [10, 18].

In fig. 3, the transverse momentum distributions of the two tagging jets and as well as the transverse momentum and pseudorapidity distributions of the third-hardest jet are shown. While the tagging jet  $p_T$  spectra agree well between VINCIA and PYTHIA with dipole recoil, differences are visible for the third-jet observables, with similar shapes but

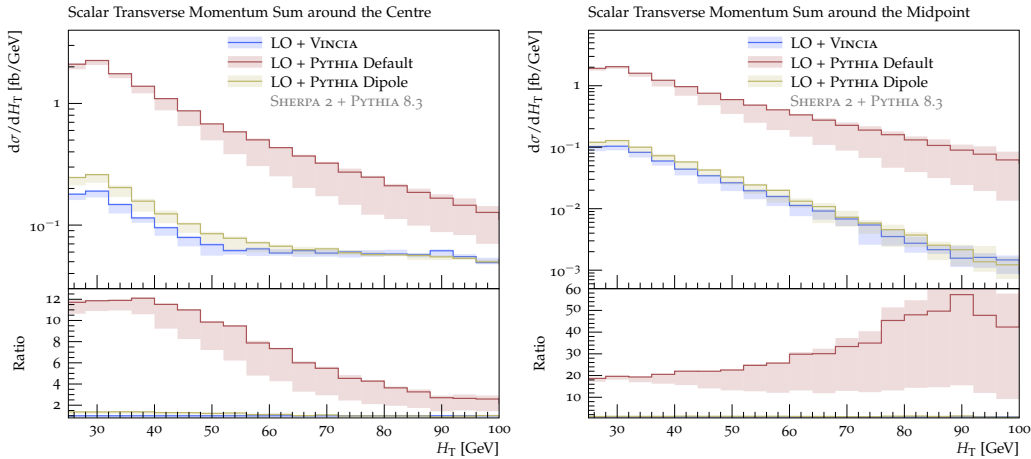


Figure 4: Scalar transverse momentum sum in the central rapidity region (*left*) and around the rapidity midpoint of the tagging jets (*right*) at LO+PS accuracy. The bands are obtained by a variation of the default shower starting scale by a factor of two.

373 a slightly larger rate produced by the PYTHIA dipole-recoil shower. The distributions  
 374 obtained with the PYTHIA default shower, on the other hand, neither agree in shape nor  
 375 in the rate with the other two. In fact, almost no suppression of radiation in the central-  
 376 rapidity region is visible and the shower radiation appears at a much higher transverse  
 377 momentum scale. The high emission rate in the default shower also implies that the  
 378 tagging jets receive much larger corrections with this shower than with the other models,  
 379 as evident from the tagging jet  $p_T$  distributions.

380 Figure 4 shows the  $H_T$  distributions in the previously defined central and midpoint  
 381 regions. As for the third-jet pseudorapidity and transverse-momentum distributions, there  
 382 is only a minor disagreement between PYTHIA dipole-recoil shower and VINCIA, while  
 383 PYTHIA’s DGLAP shower generates significantly more radiation in both regions.

384 For all observables considered here, we also note that the variation of the shower  
 385 starting scale has a much more pronounced effect on the PYTHIA default shower than on  
 386 VINCIA or on PYTHIA when the dipole-recoil option is enabled. Moreover, the starting-scale  
 387 variation affects the  $p_T$  distribution of the third jet more than it does the pseudorapidity  
 388 distribution. This indicates that, while a tailored shower starting scale for the default  
 389 shower might be able to mimic the phase space-suppression of the dipole/antenna showers  
 390 to some extent, this would not by itself be sufficient to represent the dipole-antenna  
 391 emission pattern of the third jet.

392 We close this subsection by comparing showers off our externally generated Born-level  
 393 VBF events (i.e., ones generated by SHERPA and passed to PYTHIA for showering) to show-  
 394 ers off internally generated ones (i.e., ones generated by PYTHIA’s `HiggsSM:ff2Hff(t:WW)`  
 395 and `HiggsSM:ff2Hff(t:ZZ)` processes). This is intended as a cross check for any effects  
 396 caused by differences in how PYTHIA treats external vs internal events. For instance, for  
 397 external events, the external generator is responsible not only for computing the hard  
 398 cross section but also for setting the shower starting scale, via the HDF5 `scales` dataset  
 399 (equivalent to the Les Houches `SCALUP` parameter [53,54]). For our VBF events, the choice  
 400 made in SHERPA is identical to the factorisation scale eq. (3),

$$\text{SHERPA VBF events: } \mu_{\text{PS}}^2 \equiv \mu_{\text{F}}^2 = \frac{\hat{H}_{\text{T}}^2}{4} = \frac{1}{4} \left( \sum_j p_{\text{T},j} + \sqrt{M_{\text{H}}^2 + p_{\text{T},\text{H}}^2} \right)^2.$$

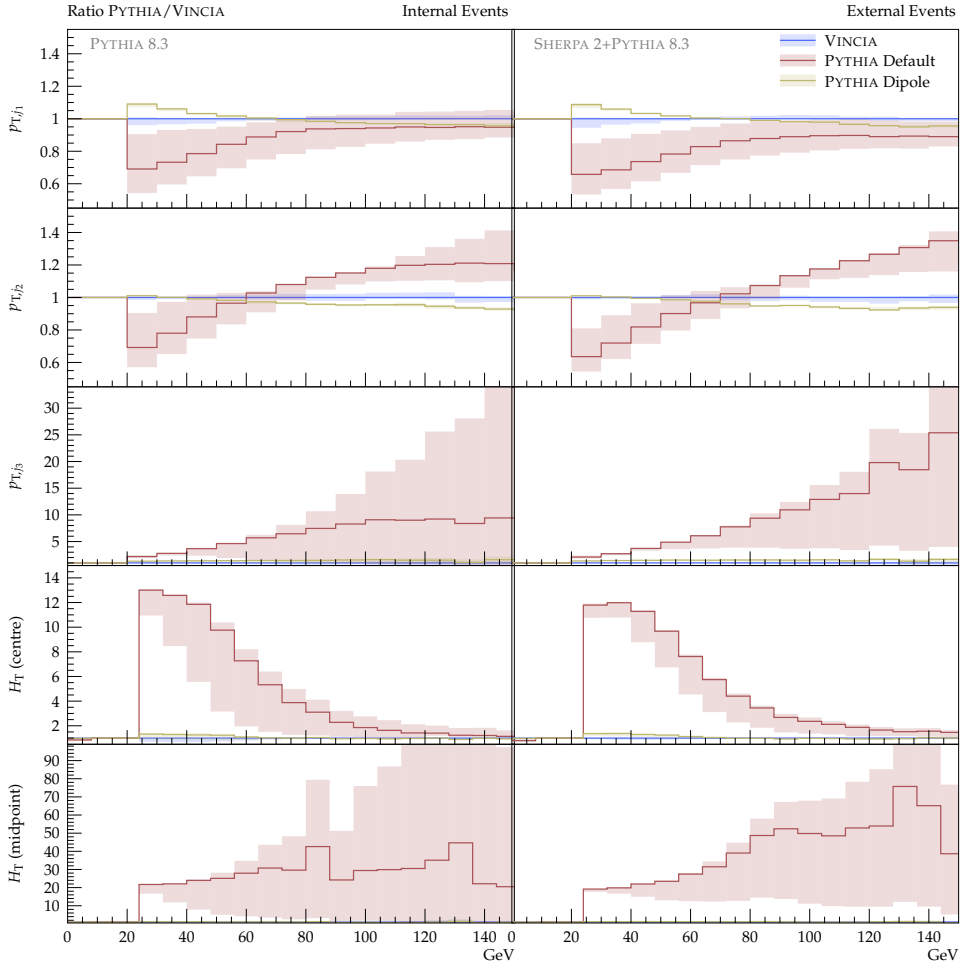


Figure 5: Ratio of PYTHIA to VINCIA at LO+PS accuracy, comparing internal (*left*) and external (*right*) events. The bands are obtained by a variation of the factorisation scale (internal events) and shower starting scale (external events) by a factor of two.

401 For internally generated VBF events, PYTHIA’s choice of the factorisation scale, and  
 402 thereby also the shower starting scale, is designed to reflect the off-shellness of the two  
 403 virtual-boson  $t$ -channel propagators, cf. eq. (5),

$$\text{PYTHIA VBF events: } \mu_{\text{PS}}^2 \equiv \mu_{\text{F}}^2 = \sqrt{m_{\text{T},V_1}^2 m_{\text{T},V_2}^2} \equiv \sqrt{(M_{V_1}^2 + p_{\text{T},q_1}^2)(M_{V_2}^2 + p_{\text{T},q_2}^2)}.$$

404 This choice ensures that the factorisation scale and shower starting scale will always be  
 405 at least of order  $M_V^2$  even when the outgoing quarks have low  $p_{\text{T}} \ll M_V$ , while for very  
 406 large  $p_{\text{T}}$  values, it asymptotes to the geometric mean of the quark  $p_{\text{T}}$  values. While  
 407 the minimum of the SHERPA choice is of the same order,  $\mathcal{O}(M_{\text{H}}) \sim \mathcal{O}(M_V)$ , the large-  
 408 transverse-momentum limit is considerably larger. The expectation is therefore that, in  
 409 the absence of matching or merging corrections, SHERPA-generated Born events will lead  
 410 to higher amounts of hard shower radiation than PYTHIA-generated ones.

411 In fig. 5, the ratio of the two PYTHIA showers to VINCIA is shown for the  $p_{\text{T}}$  and  
 412  $H_{\text{T}}$  spectra using (left) PYTHIA LO and (right) SHERPA LO events. We immediately note  
 413 that, in the low- $p_{\perp}$  limit, the excess of soft radiation generated by PYTHIA’s default shower  
 414 (red) persists in both samples. In the high- $p_{\perp}$  regions, the agreement between the simple  
 415 shower and the two dipole/antenna options (blue and yellow) tends to be best for PYTHIA’s  
 416 internal hard process. This likely originates from the lower value for the default shower

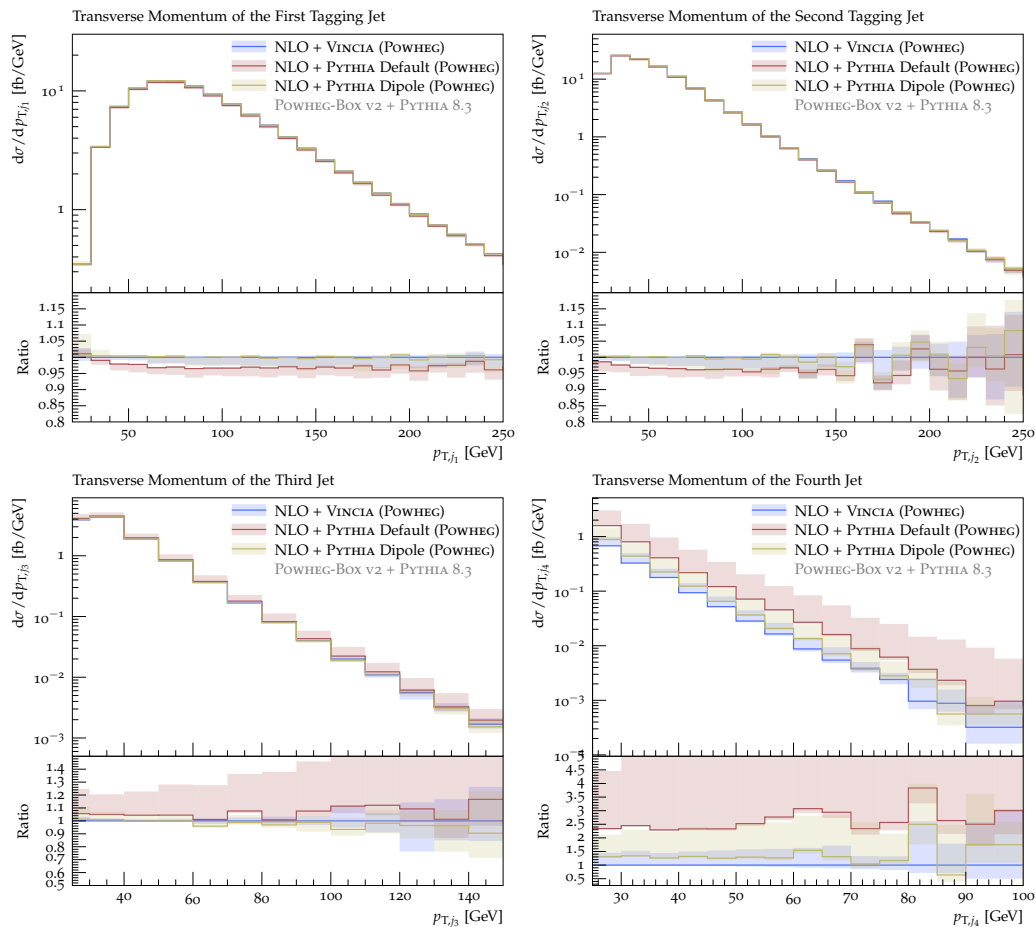


Figure 6: Transverse momentum of the first tagging jet (*top left*), second tagging jet (*top right*), third jet (*top left*), and fourth jet (*top right*) at NLO+PS accuracy in the POWHEG scheme. The bands are obtained by a variation of the hard scale in the vetoed showers as explained in the text.

417 starting scale in PYTHIA, which, as discussed above, imitates the propagator structure  
 418 of the Born process as closely as possible and hence *should* to some extent set a natural  
 419 boundary for strongly ordered propagators in the shower. For the dipole/antenna showers,  
 420 the sensitivity to the starting scale is far milder, as the relevant kinematic information is  
 421 encoded in the dipole invariant masses independently of the choice of starting scale.

### 422 3.2 Next-to-Leading Order Matched

423 In fig. 6, the POWHEG-matched transverse momentum distributions of the four hardest  
 424 jets are collected. In comparison to the LO+PS case discussed in the last section, it  
 425 is directly evident that the Born-jet  $p_T$  distributions are in good agreement between all  
 426 three shower models, including the default PYTHIA one, for which the tagging jet  $p_T$   
 427 distributions undershoot the VINCIA curve only by an approximately constant factor of  
 428 order of five per cent. After POWHEG matching, almost perfect agreement is found for the  
 429 tagging jet transverse momentum distributions obtained with VINCIA and PYTHIA with  
 430 dipole recoil, as can be seen in fig. 8. The NLO corrections are, however, slightly smaller  
 431 for the former. The scale choice of the POWHEG emission has only mild effects on all three  
 432 showers for these tagging-jet observables.

433 Good agreement is also found between all three shower models for the  $p_T$  of the third



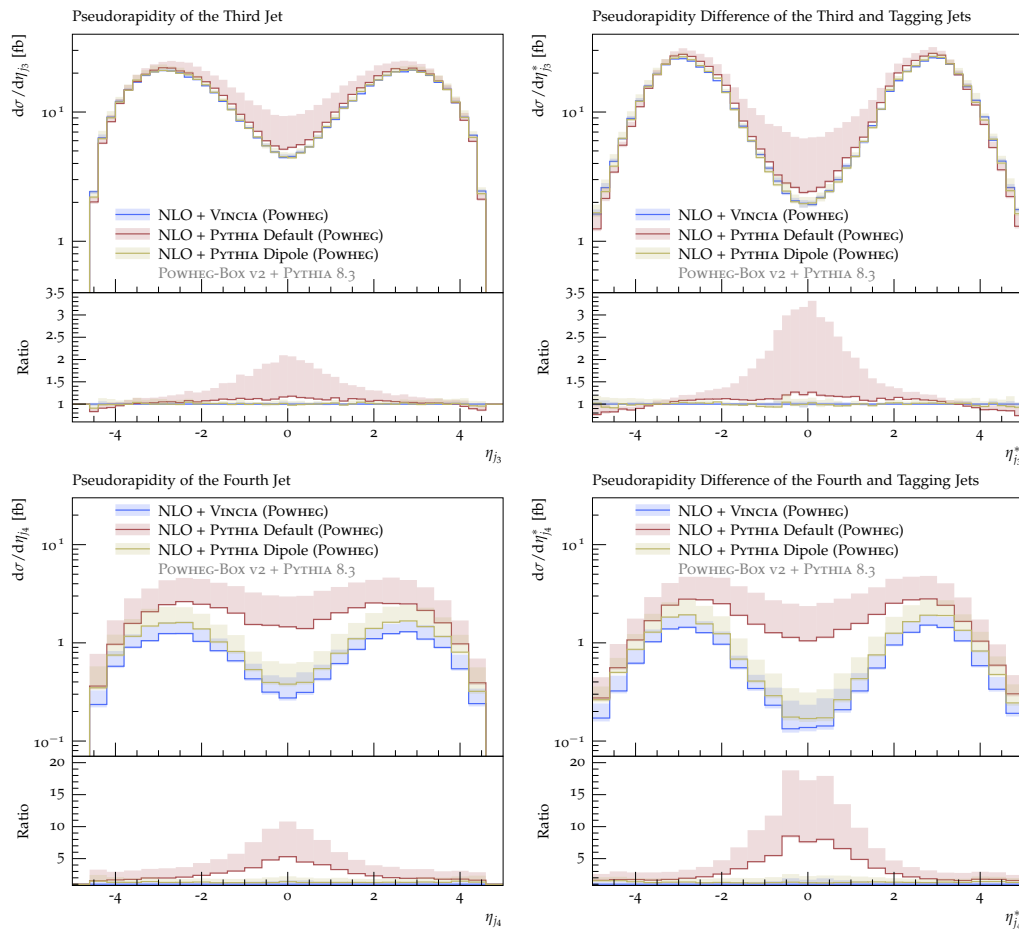


Figure 7: Pseudorapidity (*left column*) and relative rapidity to the tagging jets (*right column*) of the third jet (*top row*) and fourth jet (*bottom row*) at NLO+PS accuracy in the POWHEG scheme. The bands are obtained by a variation of the hard scale in the vetoed showers as explained in the text.

434 jet, as shown in the bottom left panel of fig. 6. It must be noted that, again in the  
 435 case of the PYTHIA default shower, this agreement is subject to appropriately vetoing  
 436 harder emissions than the POWHEG one, which requires the definition of the POWHEG  
 437 scale according to the minimal  $p_T$  in the event, corresponding to the `POWHEG:pThard =`  
 438 `2` setting, cf. section 2.3.1. Other choices again lead to too hard third jets and heavily  
 439 increased radiation in the central rapidity region, as can be inferred from the (relative)  
 440 rapidity distributions of the third jet in the top row of fig. 7, where the importance of  
 441 a judicious POWHEG scale choice is especially visible. As for the tagging jet spectra, the  
 442 agreement in both the third-jet transverse momentum and rapidity predictions between  
 443 VINCIA and the dipole-improved PYTHIA shower is almost perfect, as shown in fig. 9.  
 444 While the correction (which in this case is essentially a LO matrix-element correction)  
 445 is positive for VINCIA, it is negative for the dipole-improved PYTHIA shower. Moreover,  
 446 in the case of VINCIA, this correction affects mostly the high- $p_T$  and the central-rapidity  
 447 region, whereas for PYTHIA's dipole-improved shower, the correction is negligible at zero  
 448 rapidity but bigger (and almost) constant at larger rapidities as well as for the transverse  
 449 momentum.

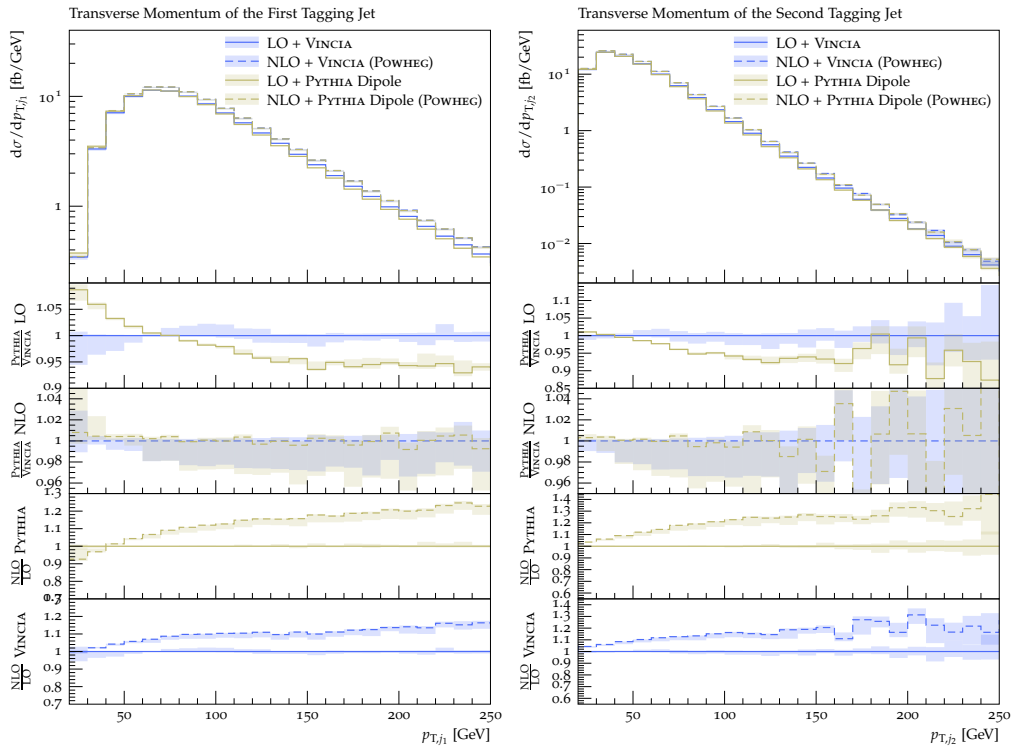


Figure 8: Detailed comparison of the PYTHIA dipole and VINCIA LO+PS and POWHEG NLO+PS predictions for the transverse momentum of the first tagging jet (*left*) and the second tagging jet (*right*).

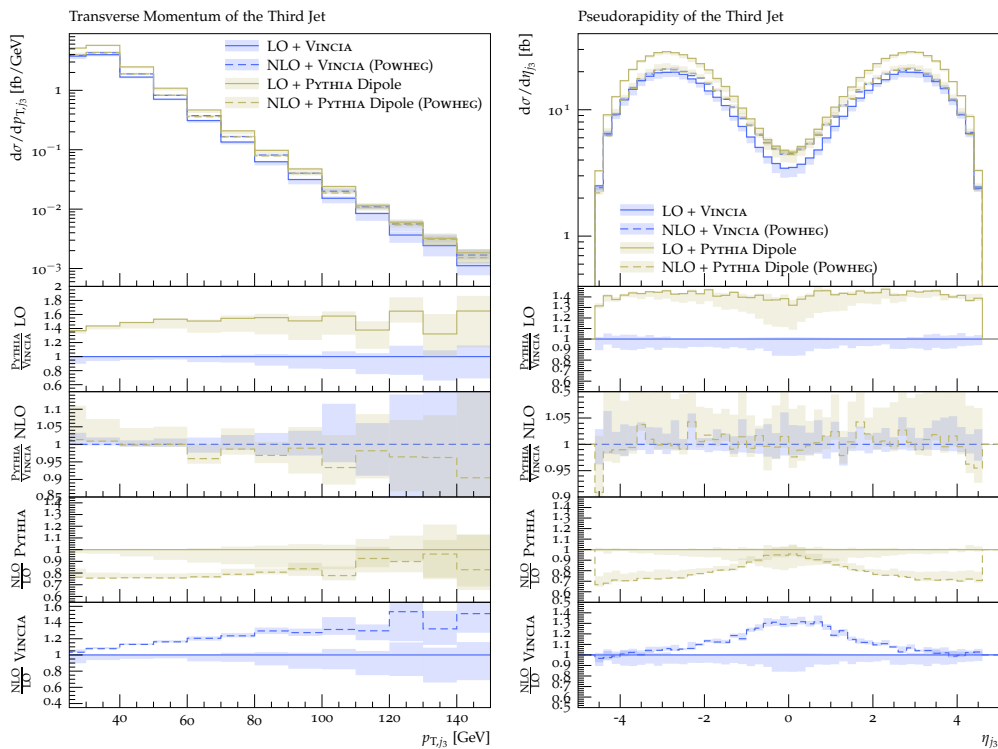


Figure 9: Detailed comparison of the PYTHIA dipole and VINCIA LO+PS and POWHEG NLO+PS predictions for the transverse momentum (*left*) and rapidity of the third jet (*right*).

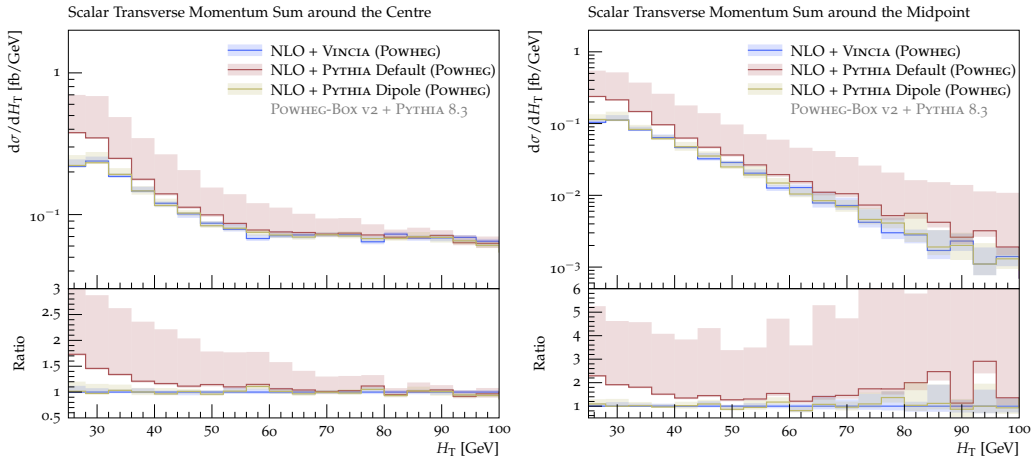


Figure 10: Scalar transverse momentum sum for  $|\eta| < 0.5$  (*left*) and around the rapidity midpoint of the tagging jets (*right*) at NLO+PS accuracy in the POWHEG scheme. The bands are obtained by a variation of the hard scale in the vetoed showers as explained in the text.

450 The bottom right pane in fig. 6 and the bottom row in fig. 7 compare the  $p_T$  and (rela-  
 451 tive) rapidity predictions of the three shower models. While again rather good agreement  
 452 in these distributions is found for the VINCIA shower and the dipole-improved PYTHIA  
 453 shower, PYTHIA’s default shower produces a harder spectrum, located more in the central  
 454 rapidity region. Here, it is worthwhile noting that for two-jet POWHEG matching, the  
 455 emission of the fourth jet is uncorrected in either of the shower models, so that the effects  
 456 visible in these distributions are solely produced by the showers.

457 Lastly, fig. 10 shows the scalar transverse momentum for  $|\eta| < 0.5$  (left) and around the  
 458 tagging jet midpoint (right) in the POWHEG NLO+PS scheme. In both distributions, the  
 459 three shower models produce similar results for  $H_T > 40$  GeV, while in the complementary  
 460 region again only VINCIA and the dipole-improved PYTHIA shower agree. In this soft region,  
 461 the default PYTHIA shower again predicts more radiation than the other two. As before,  
 462 a variation of the POWHEG scale choice leads to significant effects in the predictions of  
 463 PYTHIA’s default shower, but has only mild effects on the dipole-improved shower and  
 464 VINCIA.

### 465 3.3 Comparison of Matching and Merging

466 In figs. 11 to 13, we compare the VINCIA NLO-matched predictions presented in the last  
 467 section to an  $\mathcal{O}(\alpha_S)$  tree-level merged calculation using the CKKW-L scheme implemented  
 468 for VINCIA. For the latter, we include the exclusive zero-jet and inclusive Sudakov-weighted  
 469 1-jet predictions in the plots (dashed lines).

470 The uncertainty bands of the merged predictions (labelled VINCIA MESS  $\mathcal{O}(\alpha_S)$ ) are  
 471 obtained by a variation of the shower renormalisation scale as per section 2.2. As VINCIA’s  
 472 merging implementation reweights event samples by a ratio of the strong coupling as used  
 473 in the shower to the one used in the fixed-order calculation, this variation effectively  
 474 amounts to an intertwined scale variation of the hard process as well. The uncertainty  
 475 bands of the NLO-matched calculation are obtained by the variation of the  $p_{\perp, \text{hard}}$  scale  
 476 as in the previous section.

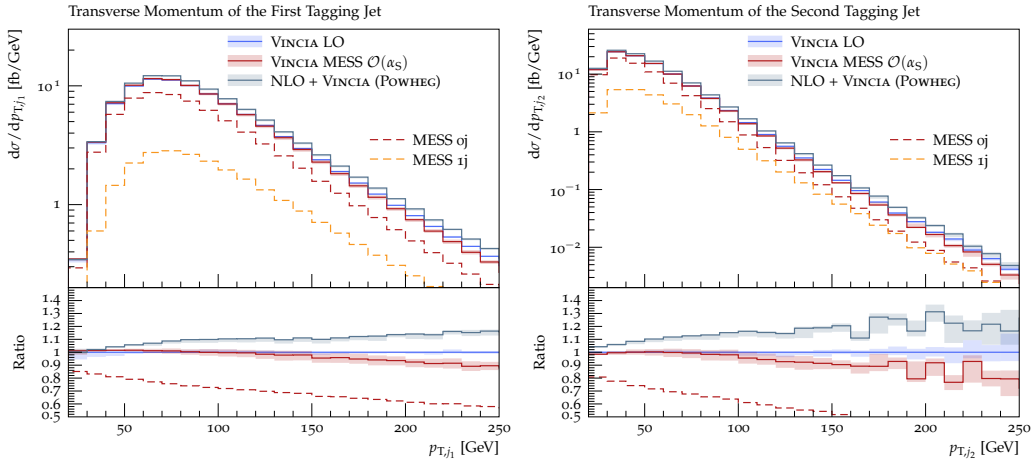


Figure 11: Comparison between LO+PS, POWHEG NLO+PS, and CKKW-L-merged predictions for the transverse momentum of the first (*left*) and second (*right*) tagging jet.

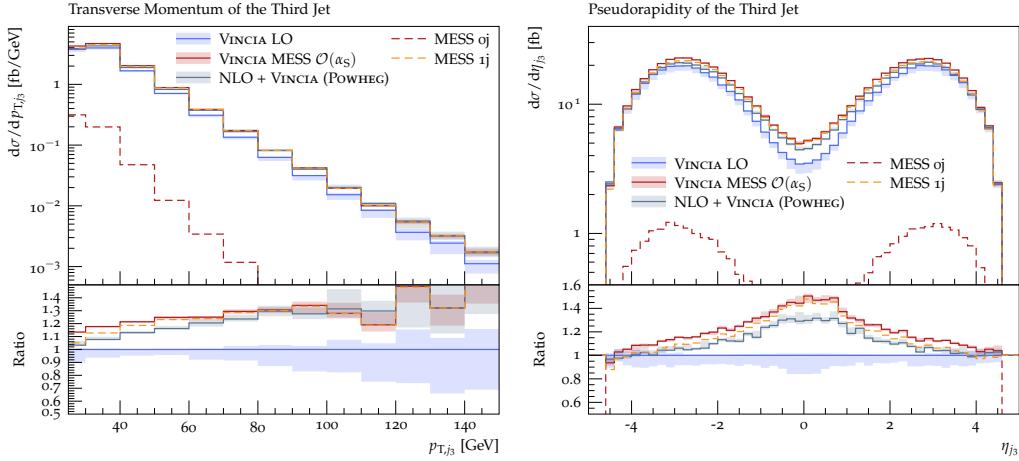


Figure 12: Comparison between LO+PS, POWHEG NLO+PS, and CKKW-L-merged predictions for the transverse momentum (*left*) and pseudorapidity (*right*) of the third jet.

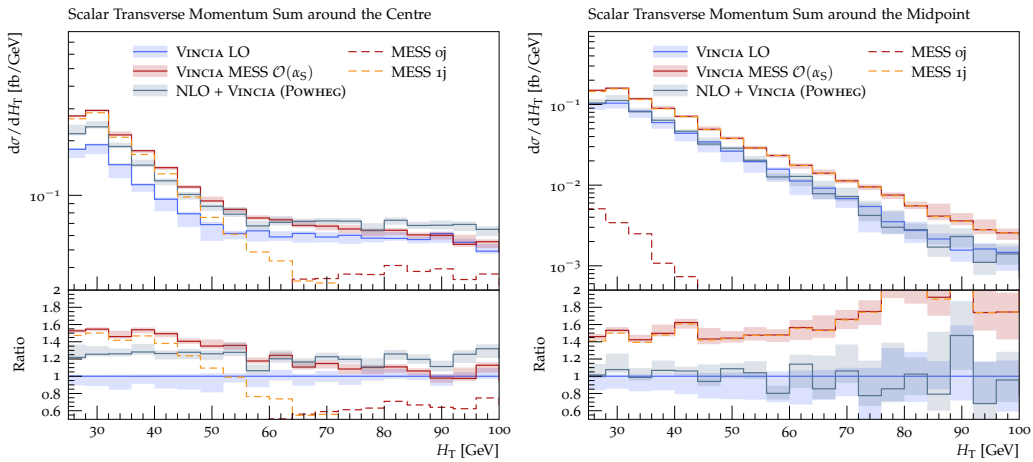


Figure 13: Comparison between LO+PS, POWHEG NLO+PS, and CKKW-L-merged predictions for the scalar transverse momentum sum for  $|\eta| < 0.5$  (*left*) and around the pseudorapidity midpoint of the tagging jets (*right*).

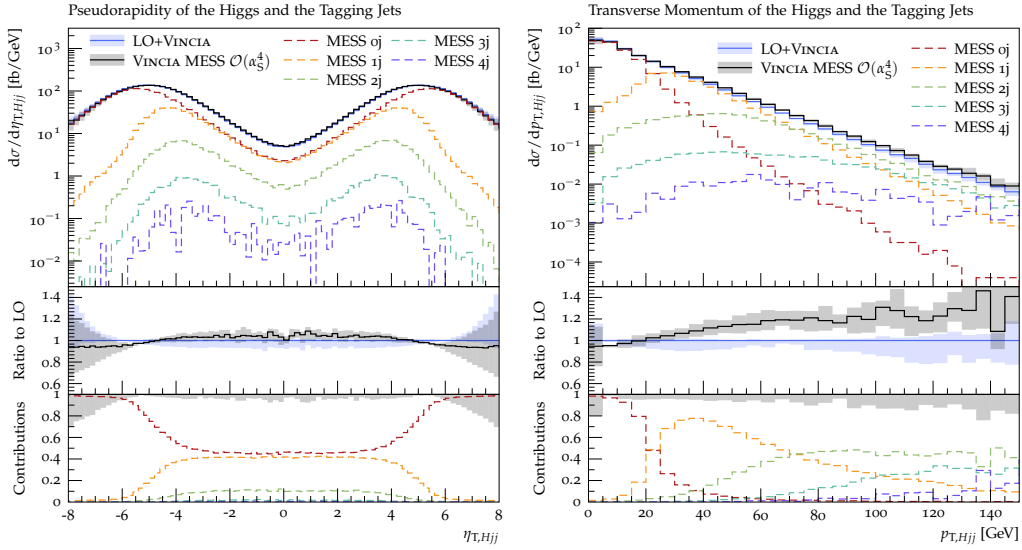


Figure 14: Tree-level merged predictions with up to four additional jets for the pseudorapidity (*left*) and transverse momentum (*right*) of the Higgs and tagging jets system.

477 Taking into account their respective accuracies, we observe good agreement between  
 478 the matched and the merged predictions for the transverse momentum and pseudorapidity  
 479 spectra. We expect the small differences that are visible to trace back mainly to the lack  
 480 of unitarity in the CKKW-L scheme. This explanation is supported by the fact that the  
 481 merged calculation overshoots the matched ones and that e.g. for the  $p_{T,j3}$  distribution,  
 482 the inclusive Sudakov-reweighted 1-jet contribution already agrees in shape and magnitude  
 483 with the matched distributions, while the exclusive zero-jet contributions only adds to the  
 484 rate, i.e overall normalisation. In addition, we wish to note again that the mismatch of the  
 485 POWHEG and VINCIA ordering variables is only treated approximately via the use of vetoed  
 486 showers, while the correct shower history is taken into account in the merged calculation.  
 487 Furthermore, we have used two different renormalisation and factorisation scales in the  
 488 two calculations. Because the renormalisation scale variation in VINCIA's merging affects  
 489 the renormalisation scale of the hard process, as alluded to above, the renormalisation  
 490 scale mismatch is covered to some degree by the scale variations in the merging.

491 The situation is different for the  $H_T$  distributions, cf. fig. 13. In the merged calculation,  
 492 more soft radiation is predicted in the central pseudorapidity region than in the matched  
 493 one. The distribution is solely governed by the one-jet sample there, while the zero-jet  
 494 sample contributes significantly above 60 GeV only. In the midpoint region, however, the  
 495 merged calculation predicts the same shape as the matched one, but with an overall bigger  
 496 rate. Barely any contribution stems from the exclusive zero-jet sample in this observable.  
 497 This confirms the properties of the two  $H_T$  observables mentioned in section 2.4. When  
 498 the observable is defined over the central rapidity region, it is sensitive to the radiation of  
 499 the third jet in the soft region, i.e. for  $H_T \lesssim 60$  GeV, but becomes sensitive to the tagging  
 500 jets in the complementary hard region, i.e. above around 60 GeV. In contrast, defining  
 501 the observable over the region around the pseudorapidity midpoint of the two tagging jets  
 502 cleans it from almost all contributions stemming from the Born configuration (only a tiny  
 503 contribution from soft radiation off the Born survives). Due to this property, the latter of  
 504 the two definitions is particularly suited in the study of the radiation pattern regarding  
 505 its coherence.

506 The comparison of NLO matching and  $\mathcal{O}(\alpha_S)$  tree-level merging provides a strong cross  
 507 check of both methods.

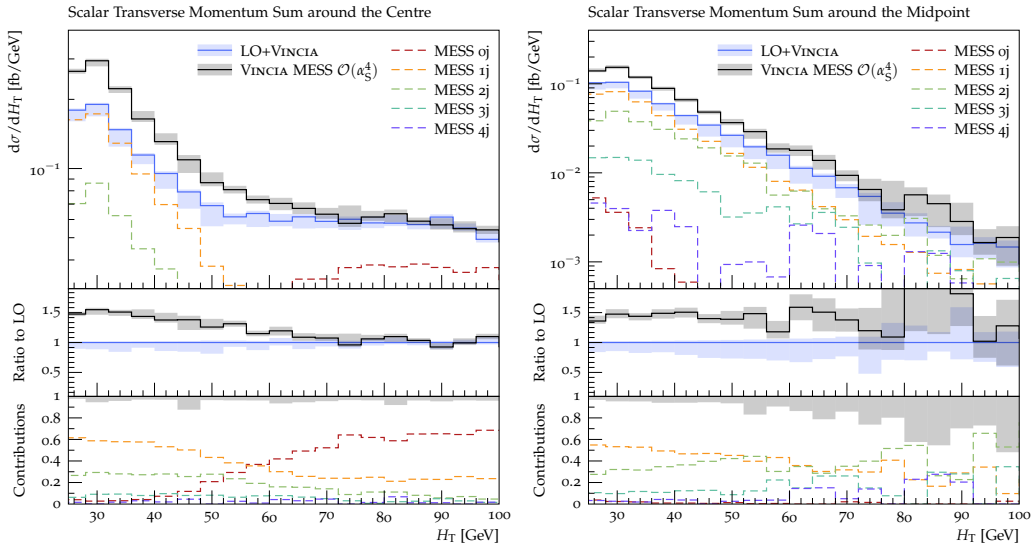


Figure 15: Tree-level merged predictions with up to four additional jets for the scalar transverse momentum sum in the central (*left*) and midpoint (*right*) pseudorapidity region.

### 508 3.4 Merged with up to Four Jets

509 In addition to the one-jet merged calculation of the last section, we here present a tree-  
 510 level merged calculation with up to four additional jets (i.e., 6 jets in total when counting  
 511 the tagging jets) using VINCIA’s CKKW-L implementation. We consider the effect of ad-  
 512 ditional hard jets on the spectra of the pseudorapidity and transverse momentum of the  
 513 Higgs plus tagging jets system as well as the herein before mentioned scalar transverse  
 514 momentum sum in the two pseudorapidity regions. The uncertainty bands of the merged  
 515 calculation shown in the figures are obtained by a variation of the renormalisation scale  
 516 prefactors  $k_R$ , c.f. section 2.2, in VINCIA’s shower and merging, again effectively represent-  
 517 ing a variation of the renormalisation scale in the hard process as well, cf. section 3.3. As  
 518 visible from fig. 15, the inclusion of additional hard jets does not change the pseudorapid-  
 519 ity spectrum, but increases the rate of the transverse momentum spectrum in the high- $p_T$   
 520 region. This correction is exactly what is expected from a multi-jet merged calculation.  
 521 The dashed lines in fig. 15 represent the different multi-jet contributions to the merged  
 522 prediction. Again as expected, the Born sample dominates in the low- $p_T$  region and the  
 523 one-jet sample in the region around 40 GeV, whereas higher multiplicities take over in  
 524 the harder regions above  $\sim 70$  GeV. It is worth highlighting, however, that, at least in  
 525 the region  $70 \text{ GeV} \lesssim p_T \lesssim 150 \text{ GeV}$ , the two-jet sample dominates with only sub-leading  
 526 corrections from the three- and four-jet samples.

527 Figure 14 shows the  $H_T$  distributions in the central and midpoint pseudorapidity re-  
 528 gions defined in section 2.4. As for the one-jet merged prediction presented in section 3.3,  
 529 the high- $H_T$  region is dominated by the Born sample, while for small  $H_T$ , the samples with  
 530 additional jets define the shape. Although all samples with additional jets contribute to  
 531 the central  $H_T$  over the full shown spectrum, the three-jet sample (denoted  $1j$  in fig. 14) is  
 532 the dominant extra-jet sample everywhere. Above approximately 60 GeV, the Born sam-  
 533 ple becomes the predominant one, highlighting again that this region is sensitive mainly  
 534 to the tagging jets. Corrections from the multi-jet merging are negligible there.

535 As before, the situation is different in the midpoint region between the two tagging  
 536 jets (right-hand pane in fig. 14). There, the Born sample has almost no impact ( $< 5\%$ )  
 537 on the  $H_T$  distribution and the one-jet sample (denoted  $1j$  in fig. 14) dominates in the



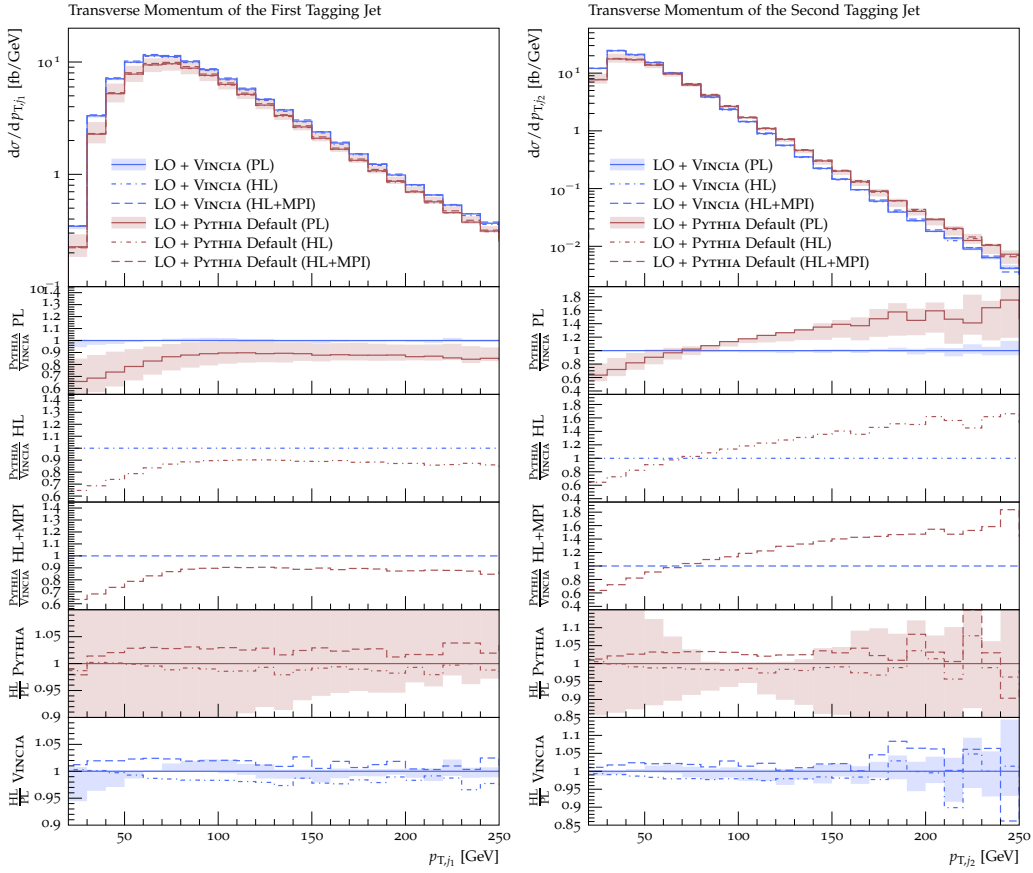


Figure 16: Detailed comparison of PYTHIA DGLAP and VINCIA LO+PS predictions at parton-level, hadron-level, and hadron-level plus MPI for the transverse momentum of the first tagging jet (*left*) and the second tagging jet (*right*).

538 region  $\lesssim 70$  GeV, while the two-jet sample (denoted  $2j$  in fig. 14) does in the region  
 539  $70$  GeV  $\lesssim H_T \lesssim 100$  GeV. This emphasises the finding of the last section that the  
 540 midpoint  $H_T$  is clean of contributions from the tagging jets and therefore more relevant  
 541 in the study of coherence effects in QCD radiation.

### 542 3.5 Hadronisation and Multi-Parton Interactions

543 Although we focused on the parton level throughout this study, we wish to close by esti-  
 544 mating the size of non-perturbative corrections arising from hadronisation, fragmentation,  
 545 and multi-parton interactions. To this end, we employ PYTHIA's string fragmentation and  
 546 interleaved MPI model [11] using the default PYTHIA [40] and VINCIA [24] tunes.

547 Figures 16 to 18 compare PYTHIA's simple shower and VINCIA predictions on the  
 548 parton level, hadron level, and hadron level with MPIs at LO+PS accuracy. As expected  
 549 from the cuts employed in our analysis, cf. section 2.4, the inclusion of non-perturbative  
 550 effects in either of the two simulations has only a negligible effect on most observables  
 551 studied here, although the discrepancy between the two showers is slightly mitigated. A  
 552 notable exception are the VINCIA predictions for the  $H_T$  in the two pseudorapidity regions  
 553 defined in section 2.4, for which the inclusion of MPIs leads to a substantial excess in  
 554 radiation in the soft region. This means, that in those regions the coherent suppression  
 555 of radiation by VINCIA is overwhelmed by the soft radiation off secondary (non-VBF-like)  
 556 interactions, at least with our set of cuts. It should be noted here that firstly, this excess

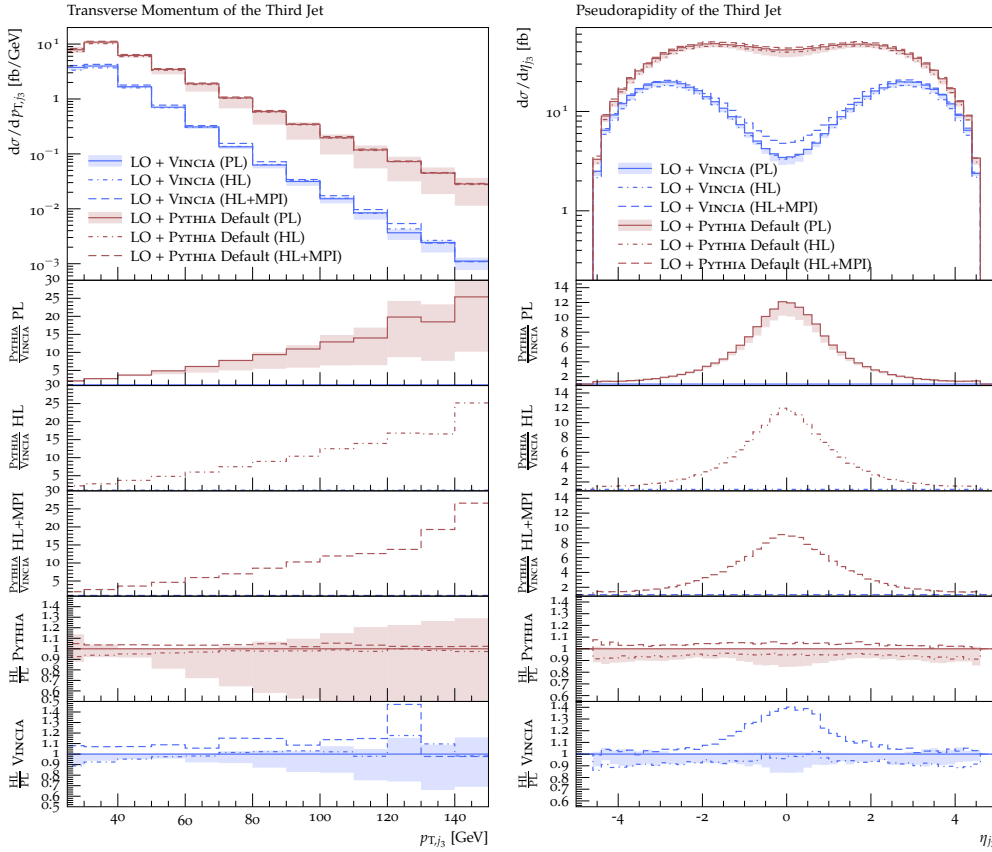


Figure 17: Detailed comparison of PYTHIA DGLAP and VINCIA LO+PS predictions at parton level, hadron level, and hadron-level plus MPI for the transverse momentum (*left*) and pseudorapidity of the third jet (*right*).

557 is not visible in the distributions obtained with PYTHIA’s simple shower, and secondly,  
 558 the discrepancy between the simple shower and VINCIA overpowers the MPI effect greatly.  
 559 As such, the inclusion of hadron-level and MPI effects emphasise that VINCIA’s antenna  
 560 shower reproduces QCD coherence effects more faithfully than PYTHIA’s simple shower.

## 561 4 Conclusion

562 We have here studied the effect of QCD radiation in VBF Higgs production, focusing in  
 563 particular on how the coherent emission patterns exhibited by this process are modelled  
 564 by various parton-shower approaches that are available in the PYTHIA event generator,  
 565 and how significant the corrections to that modelling are, from higher fixed-order matrix  
 566 elements. From a QCD point of view, the main hallmark of VBF is that gluon emission in  
 567 the central region originates from intrinsically coherent interference between initial- and  
 568 final-state radiation. This interplay is challenging to capture for DGLAP-style showers  
 569 that are anchored in the collinear limits and treat ISR and FSR separately, while it is  
 570 a quite natural element in dipole- and antenna-based formalisms, in which initial-final  
 571 colour flows enter on an equal footing with final-final and initial-initial flows. Hence we  
 572 would expect the latter (dipole/antenna-style) approaches to offer more robust and reliable  
 573 modelling of the radiation patterns in VBF than the former (DGLAP-based) approaches.

574 To this end, we have compared the VINCIA antenna shower to PYTHIA’s default (“sim-

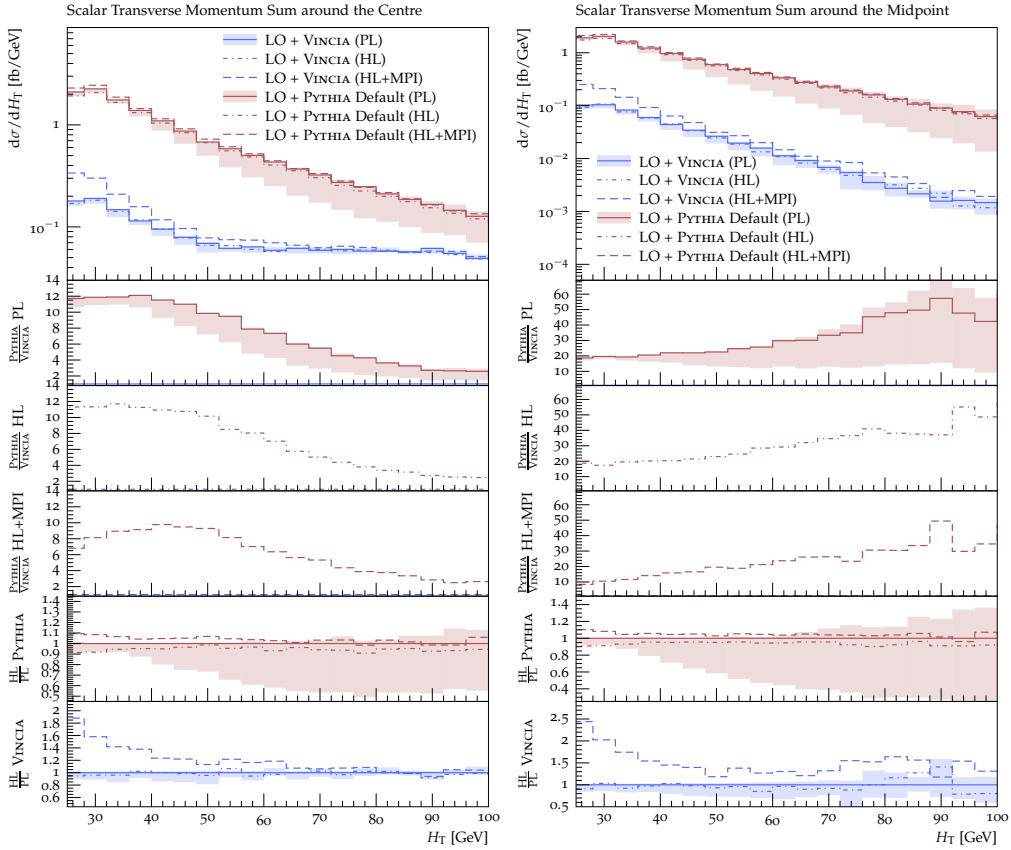


Figure 18: Detailed comparison of PYTHIA DGLAP and VINCIA LO+PS predictions at parton level predictions for the central  $H_T$  (*left*) and midpoint  $H_T$  (*right*).

575 ple”) shower, including both its (default) DGLAP and its dipole-improved option (“dipole  
 576 recoil”). We have shown that at leading order, large discrepancies pertaining to the radi-  
 577 ation of additional jets in the central rapidity regions exist between the default PYTHIA  
 578 predictions and the ones obtained with the dipole option and VINCIA, while the latter two  
 579 appear more consistent. This effect even concerns observables related to the tagging jets,  
 580 i.e. those jets which are described by the matrix element and not the shower. We have  
 581 confirmed that these findings apply to both external (LHA) and internal events.

582 After matching the showers to the NLO, these discrepancies mostly vanish for observ-  
 583 ables sensitive to the tagging jets or third jet only, while larger effects remain visible in  
 584 observables sensitive to higher jet multiplicities. These findings are largely consistent with  
 585 the ones from an earlier study [10], although it is worth highlighting that the disagreement  
 586 found for the default PYTHIA shower is fairly less pronounced here after matching it to the  
 587 NLO via the POWHEG scheme. We consider this to be an effect of a more careful treatment  
 588 of the ordering-variable mismatch between POWHEG and PYTHIA. Based on this, we rec-  
 589 ommend varying the `POWHEG:pThard` mode contained in the `PowhegHooks` classes to gain  
 590 an estimate of systematic matching uncertainties. To reduce the uncertainties pertaining  
 591 to the use of vetoed showers with POWHEG samples, a truncated and vetoed shower should  
 592 be used with both PYTHIA and VINCIA. As alluded to above, such a scheme is not (yet)  
 593 available for either of the showers considered in the present study.

594 In addition to NLO matching, we have studied the effect of including higher-multiplicity  
 595 tree-level matrix elements in the shower via the CKKW-L merging scheme in VINCIA. We  
 596 have confirmed that the NLO-matched and one-jet merged calculations lead to comparable

597 predictions for observables sensitive to the third jet. For a set of inclusive observables,  
598 we presented predictions from a tree-level merged calculation at  $\mathcal{O}(\alpha_S^4)$ . This yields cor-  
599 rections of the order of 20% in the hard tail above around 60 GeV of the transverse  
600 momentum spectrum of the Higgs-plus-tagging-jet system. Considering the mild correc-  
601 tions in the ranges studied here, it is evident that the sample with four additional jets (i.e.  
602 the 2+4-jet sample) will contribute significantly only in the very hard tails  $H_T \gg 100$  GeV  
603 and  $p_{\perp, Hjj} \gg 150$  GeV.

604 Although not the main focus of this study, we have gained a first estimate of non-  
605 perturbative corrections on the observables studied here. While we generally found only  
606 minor changes from the inclusion of hadron-level corrections, the inclusion of MPIs had  
607 a relatively more significant effect on VINCIA’s predictions than on the ones obtained  
608 with PYTHIA’s default shower. This affected the rate of radiation in soft as well as central  
609 pseudorapidity regions, i.e. precisely the regions in which VINCIA predicts a strong coherent  
610 suppression, so that the MPI contamination becomes relatively more important.

611 With this study we also proposed two new observables, the scalar transverse momentum  
612 sum in the central pseudorapidity region and around the pseudorapidity midpoint between  
613 the two tagging jets. We have shown that both of these observables are sensitive to multi-  
614 jet radiation, but highlighted that the former becomes dominated by the tagging jets in the  
615 hard region  $H_T \gtrsim 60$  GeV. As an alternative, we demonstrated that the  $H_T$  sum around  
616 the midpoint between the tagging jets is free of this contamination, with the Born sample  
617 only giving a negligible contribution. Due to the strong suppression of radiation in this  
618 region, both observables do however receive corrections from the modelling of multi-parton  
619 interactions, which would be relevant to study further.

620 While it has been considered a coherent shower before, this has been the first time that  
621 the radiation pattern of the VINCIA antenna shower was studied with a dedicated focus  
622 on its coherence. At the same time, we have here showcased NLO matching and tree-level  
623 merging methods with VINCIA, which are both publicly available as of the PYTHIA 8.306  
624 release.

## 625 Acknowledgements

626 We acknowledge support from the Monash eResearch Centre and eSolutions-Research Sup-  
627 port Services through the MonARCH HPC Cluster. This work was further partly funded  
628 by the Australian Research Council via Discovery Project DP170100708 — “Emergent  
629 Phenomena in Quantum Chromodynamics”. CTP is supported by the Monash Graduate  
630 Scholarship, the Monash International Postgraduate Research Scholarship, and the J.L.  
631 William Scholarship. This research was supported by Fermi National Accelerator Lab-  
632 oratory (Fermilab), a U.S. Department of Energy, Office of Science, HEP User Facility.  
633 Fermilab is managed by Fermi Research Alliance, LLC (FRA), acting under Contract No.  
634 DE-AC02-07CH11359.

## 635 A POWHEG+VINCIA Setup

636 As mentioned in section 2.3.1, a dedicated vetoed-shower `UserHook` for POWHEG+VINCIA  
 637 was developed as part of this work and is included in the standard PYTHIA distribution  
 638 from version 8.306 onwards. At the time of submission of this manuscript, it is included  
 639 in the file `PowhegHooksVincia.h`, in the directory `include/Pythia8Plugins/`, which also  
 640 contains the standard `PowhegHooks.h` file. (Note that these two files may be merged into  
 641 one in a future release; if so, simply omit the corresponding step below.)

642 Assuming you have a main program that is set up to run POWHEG+PYTHIA (such as the  
 643 example program `main31.cc` included with PYTHIA), the following changes (highlighted  
 644 in red) will modify it to run POWHEG+VINCIA:

- 645 • Include the `PowhegHooksVincia.h` header file:  
 646 `#include "Pythia8Plugins/PowhegHooksVincia.h"`  
 647 (you can leave any existing `#include "Pythia8Plugins/PowhegHooks.h"` state-  
 648 ment; the two will not interfere with each other).
- 649 • Replace the POWHEG+PYTHIA user hook pointer by a POWHEG+VINCIA one:  
 650 `shared_ptr<PowhegHooks> powhegHooks;`  
 651 `powhegHooks = make_shared<PowhegHooksVincia>();`  
 652 `pythia.setUserHooksPtr((UserHooksPtr)powhegHooks);`

653 In addition, the following settings should be used:

- 654 • Switch on VINCIA's showers and allow them to fill all of phase space:  
 655 `PartonShowers:model = 2 # Use Vincia's shower model.`  
 656 `Vincia:pTmaxMatch = 2 # Power showers (to be vetoed by hook).`
- 657 • Enable shower vetoes via the `PowhegHooksVincia` (same as for `PowhegHooks`):  
 658 `POWHEG:veto = 1 # Turn shower vetoes on.`
- 659 • Turn QED/EW showers and interleaved resonance decays off:  
 660 `Vincia:ewMode = 0 # Switch off QED/EW showers.`  
 661 `Vincia:interleaveResDec= off # No interleaved resonance decays.`  
 662 While enabling QED showers (`Vincia:ewMode = 1 | 2`) should not pose any prob-  
 663 lems in the matching, it is not validated (yet). We recommend against using the  
 664 EW shower (`Vincia:ewMode = 3`) with the POWHEG matching.
- 665 • Since POWHEG-BOX event samples come unpolarised, VINCIA's helicity shower should  
 666 be turned off (the helicity shower needs a polarised Born state):  
 667 `Vincia:helicityShower = off # Use helicity-averaged antennae.`  
 668 We note that VINCIA offers the possibility to polarise Born configurations using  
 669 matrix elements provided via interfaces to external generators. We have not studied  
 670 this in the present work.
- 671 • In the POWHEG-specific settings, the number of outgoing particles in the Born pro-  
 672 cess is defined as usual, e.g. =2 for the  $2 \rightarrow 2$  example in `main31.cc`, or =3 for the  
 673  $2 \rightarrow 3$  VBF-type processes studied in this work:  
 674 `POWHEG:nFinal = 3 # Number of outgoing particles in the Born process.`
- 675 • We highly recommend varying the `POWHEG:pThard` mode, for both PYTHIA and  
 676 VINCIA, to estimate matching systematics. This is how the shaded bands in most of  
 677 the plots shown in this paper were obtained.  
 678 `POWHEG:pThard = 2 # Vary (=0,=1,=2) to estimate matching systematics.`

- 679 • We also recommend checking all accepted emissions rather than only the first few:  
680 `POWHEG:vetoCount = 10000`
- 681 • The following settings are simply left at their recommended values (the same as for  
682 `main31.cmd`); see the online manual section on POWHEG for details:  
683 `POWHEG:pTemt = 0`  
684 `POWHEG:emitted = 0`  
685 `POWHEG:pTdef = 1`
- 686 • For completeness, (we note that we have anyway turned both MPI and QED showers  
687 off in this study):  
688 `POWHEG:MPIveto = 0`  
689 `POWHEG:QEDveto = 2`

690 The event files generated by POWHEG should be provided in exactly the same way as for  
691 PYTHIA+POWHEG. If the POWHEG events were generated in several separate batches, for  
692 instance, the resulting files can be read as usual, using PYTHIA’s “subruns” functionality:

```
693 ! Powheg Subruns.
694 Beams:frameType      = 4
695 Main:numberOfSubruns = 3
696 !-----
697 Main:subrun          = 0
698 Beams:LHEF           = POWHEG-BOX-V2/VBF_H/run/pwgevents-0001.lhe
699 !-----
700 Main:subrun          = 1
701 Main:LHEFskipInit    = on
702 Beams:LHEF           = POWHEG-BOX-V2/VBF_H/run/pwgevents-0002.lhe
703 !-----
704 Main:subrun          = 2
705 Main:LHEFskipInit    = on
706 Beams:LHEF           = POWHEG-BOX-V2/VBF_H/run/pwgevents-0003.lhe
```

## 707 B VINCIA CKKW-L Setup

708 Since PYTHIA version 8.304, the release is shipped with VINCIA’s own implementation of  
709 the CKKW-L merging technique, suitably modified for sector showers.

710 In the spirit of the last section, let us again assume you have a main program running  
711 CKKW-L merging with PYTHIA’s default (“simple”) shower. (We note that this is a  
712 hypothetical setup for the purpose of this study, as the default merging implementation  
713 in PYTHIA 8.3 does not handle VBF processes. An algorithmic fix is planned for PYTHIA  
714 version 8.307 or later.) The following changes are needed to alter it to run VINCIA’s  
715 CKKW-L merging instead, with changes again highlighted in red.

- 716 • Turn VINCIA and its sector showers on<sup>5</sup>:  
717 `PartonShowers:model = 2`      `# Use Vincia’s shower model.`  
718 `Vincia:sectorShowers = on`    `# Turn sector showers on.`
- 719 • Disable VINCIA components that are not (yet) handled by the merging:  
720 `Vincia:ewMode = 0`            `# Switch off QED/EW showers.`

---

<sup>5</sup>We note that as of now, sector showers are on per default in VINCIA and this flag is listed here only for completeness.



721 `Vincia:interleaveResDec= off # No interleaved resonance decays.`  
 722 `Vincia:helicityShower = off # Use helicity-averaged antennae.`  
 723 These three limitations are intended to be temporary and may be lifted in future  
 724 updates; users are encouraged to check for changes mentioning VINCIA's merging  
 725 implementation in the Update History section of PYTHIA's HTML manual in releases  
 726 from 8.307 onwards.

- 727 • Enable the merging machinery and set the merging scale definition (in this study,  
 728 all event samples were regulated by a  $k_T$  cut, so  $k_T$ -merging is turned on):

729 `Merging:doMerging = on # Turn merging machinery on.`  
 730 `Merging:doKTmerging = on # Set  $k_T$  as merging scale.`

- 731 • Set the merging scale to the desired value in GeV (note that the cuts on the event  
 732 samples should be more inclusive than the ones in the merging!):

733 `Merging:TMS = 20 # Value of the merging scale in GeV.`

- 734 • Replace the `Process` string by one obeying VINCIA's syntax, i.e. encased in curly  
 735 brackets and with whitespaces between particles, and switch the dedicated VBF  
 736 treatment on:

737 `Merging:process = { p p > h0 j j } # Define the hard process.`  
 738 `Vincia:mergeVBF = on # Enable merging in VBF systems.`

- 739 • Set the number of additional jets with respect to the Born process (e.g. for the VBF  
 740 process considered here, the number of *additional* jets is 4, while the *total* number  
 741 of jets is 6):

742 `Merging:nJetMax = 4 # Merge samples with up to 4 additional jets.`

## 743 References

- 744 [1] D. de Florian *et al.*, *Handbook of LHC Higgs Cross Sections: 4. Deciphering the*  
 745 *Nature of the Higgs Sector* **2/2017** (2016), doi:10.23731/CYRM-2017-002, 1610.  
 746 07922.
- 747 [2] F. A. Dreyer and A. Karlberg, *Vector-Boson Fusion Higgs Produc-*  
 748 *tion at Three Loops in QCD*, Phys. Rev. Lett. **117**(7), 072001 (2016),  
 749 doi:10.1103/PhysRevLett.117.072001, 1606.00840.
- 750 [3] R. V. Harlander, J. Vollinga and M. M. Weber, *Gluon-Induced Weak Boson Fusion*,  
 751 Phys. Rev. D **77**, 053010 (2008), doi:10.1103/PhysRevD.77.053010, 0801.3355.
- 752 [4] M. Cacciari, F. A. Dreyer, A. Karlberg, G. P. Salam and G. Zanderighi, *Fully Differen-*  
 753 *tial Vector-Boson-Fusion Higgs Production at Next-to-Next-to-Leading Order*, Phys.  
 754 Rev. Lett. **115**(8), 082002 (2015), doi:10.1103/PhysRevLett.115.082002, [Erratum:  
 755 Phys.Rev.Lett. 120, 139901 (2018)], 1506.02660.
- 756 [5] J. Cruz-Martinez, T. Gehrmann, E. W. N. Glover and A. Huss, *Second-order QCD*  
 757 *effects in Higgs boson production through vector boson fusion*, Phys. Lett. B **781**, 672  
 758 (2018), doi:10.1016/j.physletb.2018.04.046, 1802.02445.
- 759 [6] T. Liu, K. Melnikov and A. A. Penin, *Nonfactorizable QCD Effects in Higgs Bo-*  
 760 *son Production via Vector Boson Fusion*, Phys. Rev. Lett. **123**(12), 122002 (2019),  
 761 doi:10.1103/PhysRevLett.123.122002, 1906.10899.

- 762 [7] M. Ciccolini, A. Denner and S. Dittmaier, *Electroweak and QCD corrections to Higgs*  
763 *production via vector-boson fusion at the LHC*, Phys. Rev. D **77**, 013002 (2008),  
764 doi:10.1103/PhysRevD.77.013002, 0710.4749.
- 765 [8] B. Jäger, F. Schissler and D. Zeppenfeld, *Parton-shower effects on Higgs boson*  
766 *production via vector-boson fusion in association with three jets*, JHEP **07**, 125 (2014),  
767 doi:10.1007/JHEP07(2014)125, 1405.6950.
- 768 [9] A. Buckley *et al.*, *A comparative study of Higgs boson production from vector-boson*  
769 *fusion* (2021), 2105.11399.
- 770 [10] B. Jäger, A. Karlberg, S. Plätzer, J. Scheller and M. Zaro, *Parton-shower effects*  
771 *in Higgs production via Vector-Boson Fusion*, Eur. Phys. J. C **80**(8), 756 (2020),  
772 doi:10.1140/epjc/s10052-020-8326-7, 2003.12435.
- 773 [11] T. Sjöstrand and P. Z. Skands, *Transverse-momentum-ordered showers and inter-*  
774 *leaved multiple interactions*, Eur. Phys. J. C **39**, 129 (2005), doi:10.1140/epjc/s2004-  
775 02084-y, hep-ph/0408302.
- 776 [12] R. Corke and T. Sjöstrand, *Interleaved Parton Showers and Tuning Prospects*, JHEP  
777 **03**, 032 (2011), doi:10.1007/JHEP03(2011)032, 1011.1759.
- 778 [13] T. Sjöstrand, S. Ask, J. R. Christiansen, R. Corke, N. Desai, P. Ilten, S. Mrenna,  
779 S. Prestel, C. O. Rasmussen and P. Z. Skands, *An introduction to PYTHIA 8.2*,  
780 Comput. Phys. Commun. **191**, 159 (2015), doi:10.1016/j.cpc.2015.01.024, 1410.3012.
- 781 [14] J. Alwall, R. Frederix, S. Frixione, V. Hirschi, F. Maltoni, O. Mattelaer, H. S. Shao,  
782 T. Stelzer, P. Torrielli and M. Zaro, *The automated computation of tree-level and*  
783 *next-to-leading order differential cross sections, and their matching to parton shower*  
784 *simulations*, JHEP **07**, 079 (2014), doi:10.1007/JHEP07(2014)079, 1405.0301.
- 785 [15] S. Alioli, P. Nason, C. Oleari and E. Re, *A general framework for implementing NLO*  
786 *calculations in shower Monte Carlo programs: the POWHEG BOX*, JHEP **06**, 043  
787 (2010), doi:10.1007/JHEP06(2010)043, 1002.2581.
- 788 [16] B. Cabouat and T. Sjöstrand, *Some Dipole Shower Studies*, Eur. Phys. J. C **78**(3),  
789 226 (2018), doi:10.1140/epjc/s10052-018-5645-z, 1710.00391.
- 790 [17] J. Bellm *et al.*, *Herwig 7.0/Herwig++ 3.0 release note*, Eur. Phys. J. C **76**(4), 196  
791 (2016), doi:10.1140/epjc/s10052-016-4018-8, 1512.01178.
- 792 [18] M. Rauch and S. Plätzer, *Parton Shower Matching Systematics in Vector-Boson-*  
793 *Fusion WW Production*, Eur. Phys. J. C **77**(5), 293 (2017), doi:10.1140/epjc/s10052-  
794 017-4860-3, 1605.07851.
- 795 [19] D. Buarque *et al.*, *Vector Boson Scattering Processes: Status and Prospects* (2021),  
796 2106.01393.
- 797 [20] G. Aad *et al.*, *Measurements of Higgs Bosons Decaying to Bottom Quarks from*  
798 *Vector Boson Fusion Production with the ATLAS Experiment at  $\sqrt{s} = 13$  TeV* (2020),  
799 2011.08280.
- 800 [21] G. Aad *et al.*, *Search for Higgs boson production in association with a high-energy*  
801 *photon via vector-boson fusion with decay into bottom quark pairs at  $\sqrt{s}=13$  TeV with*  
802 *the ATLAS detector* (2020), 2010.13651.

- 803 [22] A. M. Sirunyan *et al.*, *Search for invisible decays of a Higgs boson produced through*  
804 *vector boson fusion in proton-proton collisions at  $\sqrt{s} = 13$  TeV*, Phys. Lett. B **793**,  
805 520 (2019), doi:10.1016/j.physletb.2019.04.025, 1809.05937.
- 806 [23] A. M. Sirunyan *et al.*, *Measurements of Higgs boson production cross sections and*  
807 *couplings in the diphoton decay channel at  $\sqrt{s} = 13$  TeV* (2021), 2103.06956.
- 808 [24] H. Brooks, C. T. Preuss and P. Skands, *Sector Showers for Hadron Collisions*, JHEP  
809 **07**, 032 (2020), doi:10.1007/JHEP07(2020)032, 2003.00702.
- 810 [25] S. Catani, F. Krauss, R. Kuhn and B. R. Webber, *QCD matrix elements + par-*  
811 *ton showers*, JHEP **11**, 063 (2001), doi:10.1088/1126-6708/2001/11/063, hep-ph/  
812 0109231.
- 813 [26] L. Lönnblad, *Correcting the color dipole cascade model with fixed order matrix ele-*  
814 *ments*, JHEP **05**, 046 (2002), doi:10.1088/1126-6708/2002/05/046, hep-ph/0112284.
- 815 [27] L. Lönnblad and S. Prestel, *Matching Tree-Level Matrix Elements with Interleaved*  
816 *Showers*, JHEP **03**, 019 (2012), doi:10.1007/JHEP03(2012)019, 1109.4829.
- 817 [28] H. Brooks and C. T. Preuss, *Efficient multi-jet merging with the Vincia sector shower*,  
818 Comput. Phys. Commun. **264**, 107985 (2021), doi:10.1016/j.cpc.2021.107985, 2008.  
819 09468.
- 820 [29] E. Bothmann *et al.*, *Event Generation with Sherpa 2.2*, SciPost Phys. **7**(3), 034  
821 (2019), doi:10.21468/SciPostPhys.7.3.034, 1905.09127.
- 822 [30] S. Höche, S. Prestel and H. Schulz, *Simulation of Vector Boson Plus Many Jet*  
823 *Final States at the High Luminosity LHC*, Phys. Rev. D **100**(1), 014024 (2019),  
824 doi:10.1103/PhysRevD.100.014024, 1905.05120.
- 825 [31] S. Dulat, T.-J. Hou, J. Gao, M. Guzzi, J. Huston, P. Nadolsky, J. Pumplin,  
826 C. Schmidt, D. Stump and C. P. Yuan, *New parton distribution functions from a*  
827 *global analysis of quantum chromodynamics*, Phys. Rev. D **93**(3), 033006 (2016),  
828 doi:10.1103/PhysRevD.93.033006, 1506.07443.
- 829 [32] A. Buckley, J. Ferrando, S. Lloyd, K. Nordström, B. Page, M. Rüfenacht,  
830 M. Schönherr and G. Watt, *LHAPDF6: parton density access in the LHC precision*  
831 *era*, Eur. Phys. J. C **75**, 132 (2015), doi:10.1140/epjc/s10052-015-3318-8, 1412.7420.
- 832 [33] R. D. Ball *et al.*, *Parton distributions with LHC data*, Nucl. Phys. B **867**, 244 (2013),  
833 doi:10.1016/j.nuclphysb.2012.10.003, 1207.1303.
- 834 [34] R. D. Ball, V. Bertone, S. Carrazza, L. Del Debbio, S. Forte, A. Guffanti, N. P.  
835 Hartland and J. Rojo, *Parton distributions with QED corrections*, Nucl. Phys. B  
836 **877**, 290 (2013), doi:10.1016/j.nuclphysb.2013.10.010, 1308.0598.
- 837 [35] T. Gleisberg and S. Hoeche, *Comix, a new matrix element generator*, JHEP **12**, 039  
838 (2008), doi:10.1088/1126-6708/2008/12/039, 0808.3674.
- 839 [36] P. Nason, *A New method for combining NLO QCD with shower Monte Carlo algo-*  
840 *rithms*, JHEP **11**, 040 (2004), doi:10.1088/1126-6708/2004/11/040, hep-ph/0409146.
- 841 [37] S. Frixione, P. Nason and C. Oleari, *Matching NLO QCD computations with Parton*  
842 *Shower simulations: the POWHEG method*, JHEP **11**, 070 (2007), doi:10.1088/1126-  
843 6708/2007/11/070, 0709.2092.

- 844 [38] P. Nason and C. Oleari, *NLO Higgs boson production via vector-boson fusion matched*  
845 *with shower in POWHEG*, JHEP **02**, 037 (2010), doi:10.1007/JHEP02(2010)037,  
846 0911.5299.
- 847 [39] P. Skands, B. Webber and J. Winter, *QCD Coherence and the Top Quark Asymmetry*,  
848 JHEP **07**, 151 (2012), doi:10.1007/JHEP07(2012)151, 1205.1466.
- 849 [40] P. Skands, S. Carrazza and J. Rojo, *Tuning PYTHIA 8.1: the Monash 2013 Tune*,  
850 Eur. Phys. J. C **74**(8), 3024 (2014), doi:10.1140/epjc/s10052-014-3024-y, 1404.5630.
- 851 [41] S. Amoroso *et al.*, *Les Houches 2019: Physics at TeV Colliders: Standard Model*  
852 *Working Group Report*, In *11th Les Houches Workshop on Physics at TeV Colliders:*  
853 *PhysTeV Les Houches* (2020), 2003.01700.
- 854 [42] S. Catani, B. R. Webber and G. Marchesini, *QCD coherent branching and semi-*  
855 *inclusive processes at large  $x$* , Nucl. Phys. B **349**, 635 (1991), doi:10.1016/0550-  
856 3213(91)90390-J.
- 857 [43] S. Hoeche, F. Krauss, M. Schönherr and F. Siegert, *A critical appraisal of NLO+PS*  
858 *matching methods*, JHEP **09**, 049 (2012), doi:10.1007/JHEP09(2012)049, 1111.1220.
- 859 [44] P. Nason and B. Webber, *Next-to-Leading-Order Event Generators*, Ann. Rev. Nucl.  
860 Part. Sci. **62**, 187 (2012), doi:10.1146/annurev-nucl-102711-094928, 1202.1251.
- 861 [45] R. Corke and T. Sjöstrand, *Improved Parton Showers at Large Transverse Momenta*,  
862 Eur. Phys. J. C **69**, 1 (2010), doi:10.1140/epjc/s10052-010-1409-0, 1003.2384.
- 863 [46] T. Plehn, D. Rainwater and P. Z. Skands, *Squark and gluino production with jets*,  
864 Phys. Lett. B **645**, 217 (2007), doi:10.1016/j.physletb.2006.12.009, hep-ph/0510144.
- 865 [47] S. Gieseke, P. Stephens and B. Webber, *New formalism for QCD parton showers*,  
866 JHEP **12**, 045 (2003), doi:10.1088/1126-6708/2003/12/045, hep-ph/0310083.
- 867 [48] P. Nason and C. Oleari, *Generation cuts and Born suppression in POWHEG* (2013),  
868 1303.3922.
- 869 [49] M. Cacciari, G. P. Salam and G. Soyez, *The anti- $k_t$  jet clustering algorithm*, JHEP  
870 **04**, 063 (2008), doi:10.1088/1126-6708/2008/04/063, 0802.1189.
- 871 [50] M. Cacciari, G. P. Salam and G. Soyez, *FastJet User Manual*, Eur. Phys. J. C **72**,  
872 1896 (2012), doi:10.1140/epjc/s10052-012-1896-2, 1111.6097.
- 873 [51] A. Buckley, J. Butterworth, D. Grellscheid, H. Hoeth, L. Lönnblad, J. Monk,  
874 H. Schulz and F. Siegert, *Rivet user manual*, Comput. Phys. Commun. **184**, 2803  
875 (2013), doi:10.1016/j.cpc.2013.05.021, 1003.0694.
- 876 [52] C. Bierlich *et al.*, *Robust Independent Validation of Experiment and Theory: Rivet*  
877 *version 3*, SciPost Phys. **8**, 026 (2020), doi:10.21468/SciPostPhys.8.2.026, 1912.  
878 05451.
- 879 [53] E. Boos *et al.*, *Generic User Process Interface for Event Generators*, In *2nd Les*  
880 *Houches Workshop on Physics at TeV Colliders* (2001), hep-ph/0109068.
- 881 [54] J. Alwall *et al.*, *A Standard format for Les Houches event files*, Comput. Phys.  
882 Commun. **176**, 300 (2007), doi:10.1016/j.cpc.2006.11.010, hep-ph/0609017.